

Galaxy Zoo: Stronger bars facilitate quenching in star forming galaxies

Tobias Geron¹★, R. J. Smethurst¹, Chris Lintott¹, Sandor Kruk²,
Karen L. Masters³, Brooke Simmons⁴, David V. Stark³

¹*Oxford Astrophysics, Department of Physics, University of Oxford, Denys Wilkinson Building, Keble Road, Oxford, OX1 3RH, UK*

²*European Space Agency, ESTEC, Keplerlaan 1, NL-2201 AZ, Noordwijk, The Netherlands*

³*Haverford College, Department of Physics and Astronomy, 370 Lancaster Avenue, Haverford, Pennsylvania 19041, USA*

⁴*Department of Physics, Lancaster University, Lancaster, LA1 4YB, UK*

Accepted XXX. Received YYY; in original form ZZZ

ABSTRACT

We have used Galaxy Zoo DECaLS (GZD) to study strong and weak bars in disk galaxies. Out of the 314,000 galaxies in GZD, we created a volume-limited sample ($0.01 < z < 0.05$, $M_r < -18.96$) which contains 1,867 galaxies with reliable volunteer bar classifications in the ALFALFA footprint. In keeping with previous Galaxy Zoo surveys (such as GZ2), the morphological classifications from GZD agree well with previous morphological surveys. GZD considers galaxies to either have a strong bar (15.5%), a weak bar (28.1%) or no bar (56.4%), based on volunteer classifications on images obtained from the DECaLS survey. This places GZD in a unique position to assess differences between strong and weak bars. We find that the strong bar fraction is typically higher in quiescent galaxies than in star forming galaxies, while the weak bar fraction is similar. Moreover, we have found that strong bars facilitate the quenching process in star forming galaxies, finding higher fibre SFRs, lower gas masses and shorter depletion timescales in these galaxies compared to unbarred galaxies. However, we also found that any differences between strong and weak bars disappear when controlling for bar length. Based on this, we conclude that weak and strong bars are not fundamentally different phenomena. Instead, we propose that there is a continuum of bar types, which varies from ‘weakest’ to ‘strongest’.

Key words: galaxies: general – galaxies: bar – galaxies: evolution – galaxies: structure – galaxies: star formation

1 INTRODUCTION

Since the development of the morphological classification scheme for galaxies (Hubble 1926), spiral galaxies have been divided into two subclasses depending on whether the galaxy was observed to have a bar (SB) or to be unbarred (SA). This scheme is still used (Buta et al. 2007; Buta 2011), albeit in modified form (Hubble 1936; Sandage 1961; de Vaucouleurs 1959, 1963; de Vaucouleurs et al. 1991). One of the most important changes was the introduction of three subclasses: unbarred (SA), strongly barred (SB) and weakly barred (SAB, de Vaucouleurs 1959, 1963). The latter subclass was supposed to be an intermediate class between unbarred and strongly barred, with SAB bars having a length and contrast intermediate between SA and SB bars. Strong bars were typically long and obvious, whereas weak bars are small and faint (de Vaucouleurs 1959, 1963).

It is known that a bar can funnel gas to the centre of galaxy and

move angular momentum outwards (Sorensen et al. 1976; Athanassoula 1992b; Davoust & Contini 2004; Athanassoula et al. 2013; Villa-Vargas et al. 2010; Vera et al. 2016; Spinoso et al. 2017; George et al. 2019) and thus influence its host galaxy through slow or “secular” evolution (Kormendy & Kennicutt 2004; Cheung et al. 2013). It has been suggested before that a bar could play an important role in quenching its host (Kormendy & Kennicutt 2004; Masters et al. 2011; Kruk et al. 2018; Fraser-McKelvie et al. 2020), although the final mechanism by which the gas is depleted and the galaxy quenches is poorly understood. Studies have shown that the likelihood of hosting a bar increases in more massive, redder and gas-poor galaxies (i.e., typical quiescent galaxies, Masters et al. 2012; Cervantes Sodi 2017; Vera et al. 2016; Fraser-McKelvie et al. 2020). However, it is unclear whether the bar helps to quench those galaxies or if it is easier to form a bar in a quenched galaxy (Masters et al. 2012).

There are many theories of how bar quenching might proceed. Some suggest that after the inflow of gas to the centre due to the bar, the gas will trigger a starburst. This increases the rate of gas

★ E-mail: tobias.geron@physics.ox.ac.uk (TG)

consumption, facilitating the quenching process (Alonso-Herrero & Knapen 2001; Sheth et al. 2005; Jogee et al. 2005; Hunt et al. 2008; Carles et al. 2016). Alternatively, the gas can become too dynamically hot for star formation (by increased velocity dispersion or shear), which quenches the host galaxy (Zurita et al. 2004; Haywood et al. 2016; Khoperskov et al. 2018; Athanassoula 1992b; Reynaud & Downes 1998; Sheth et al. 2000).

The simulations of Athanassoula et al. (2013) have demonstrated that bars tend to form later if the gas fraction is high. Some observations show higher SFE/SFR in barred regions (Alonso-Herrero & Knapen 2001; Hunt et al. 2008; Coelho & Gadotti 2011; Hirota et al. 2014; Janowiecki et al. 2020; Magaña-Serrano et al. 2020; Lin et al. 2020), while others observe lower SFR/SFE (Mose et al. 2010; Yajima et al. 2019; Maeda et al. 2020). Sheth et al. (2000) has shown a lower SFR in the region between the centre and bar ends, but higher in the very centre. The observations of James & Percival (2018) suggest a ‘star formation desert’ within the galaxy, where a strong bar suppresses SF by sweeping over it. This is also observed by Spinoso et al. (2017); George et al. (2019); Newnham et al. (2020). These observations demonstrate that bar quenching is localised in the disk region within the bar radius. Watanabe et al. (2011) found similar SFE in the bar and disk region, but an elevated SFE in the bar-end region. These simulations and observations show that barred structures have a definite effect on their host, especially in terms of SFR.

A reliable and fast method to identify bars and quantify their strength is essential to study them. However, constructing a precise definition of bar strength is not straightforward, even though the idea is intuitive (Athanassoula 2003). Many methods to measure bar strength have been proposed. For example, de Vaucouleurs (1959) initially used morphological arguments to differentiate between weak and strong bars; bars in weakly barred galaxies are less evident and shorter, whereas bars in strongly barred galaxies are long and obvious. In the catalogue of detailed visual morphological classifications of Nair & Abraham (2010a), a bar is defined to be strong if it appears to dominate the light distribution, whereas only a small proportion of the total flux of the galaxy should be found in a weak bar. Other popular methods to measure bar strength include using the $m = 2$ Fourier mode (Athanassoula 2003; García-Gómez et al. 2017) or using isophotes. It has been shown that both the maximum ellipticity of the bar isophote (Athanassoula 1992a; Laurikainen & Salo 2002; Erwin 2004) and the boxiness of the isophotes (Gadotti 2011) approximate bar strength. Estimations of the bar torque have also been used before (Combes & Sanders 1981; Buta & Block 2001; Laurikainen & Salo 2002; Speltinx et al. 2008). Hoyle et al. (2011); Guo et al. (2019) have found a positive correlation between the bar length and bar strength. Finally, previous work has suggested that weak and strong bars have different surface brightness profiles. Weaker bars have exponential profiles, whereas stronger bars have flatter profiles (Elmegreen & Elmegreen 1985; Elmegreen et al. 1996; Kim et al. 2015; Kruk et al. 2018). There are numerous methods to detect and characterize bars, but there is no general consensus among the community on which method is preferable or on the absolute definition of strong and weak bars.

A novel method to approach this problem was investigated in Galaxy Zoo 2 (hereafter GZ2), where citizen scientists were asked to classify SDSS images (York et al. 2000; Blanton et al. 2017) according to a decision tree structure (please refer to Lintott et al. (2008, 2011); Willett et al. (2013) for more details). Whether or not the galaxy had a bar was one question in this decision tree. A total of ~300,000 galaxies were classified using more than 16 million

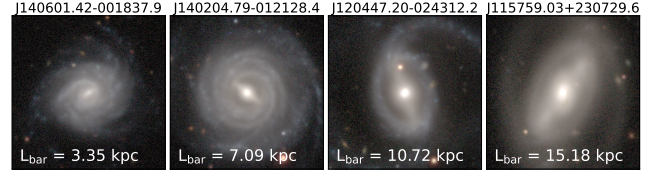


Figure 1. DECaLS postage stamps (72x72 arcsec) of low redshift ($0.01 < z < 0.025$) of galaxies with various bar sizes. See Section 2.4 for information about the bar length measurements. This image showcases the variety of bar shapes and sizes.

morphological classifications. It has been shown that GZ2 agrees well with morphological catalogues based on expert classifications (Willett et al. 2013) and the GZ2 bar classifications have been used to study bars before (Hoyle et al. 2011; Masters et al. 2011, 2012; Skibba et al. 2012; Cheung et al. 2013; Melvin et al. 2014; Simmons et al. 2014; Cheung et al. 2015; Galloway et al. 2015; Kruk et al. 2017, 2018, 2019). Nevertheless, it must be noted that GZ2 only asked whether or not the galaxy had a bar and did not attempt to measure bar strength directly. However, as visualised in Figure 1, bars come in various shapes and sizes, all with varying impacts on their host galaxy. This issue is addressed in Galaxy Zoo DECaLS (GZD), the new version of Galaxy Zoo. In GZD, volunteers chose whether the galaxy had no bar, a weak bar or a strong bar (see Section 2.1). Images from the Dark Energy Camera Legacy Survey (DECaLS) were used to complement this more detailed question, as DECaLS is a much deeper survey than SDSS (DECaLS has a median 5σ point source depth of $r = 23.6$, whereas SDSS DR7 is 95% complete to $r = 22.2$, Abazajian et al. 2009; Dey et al. 2019). DECaLS uses the Dark Energy Camera (DECam, Flaugher et al. 2015) on the 4m Blanco telescope at the Cerro Tololo Inter-American Observatory. For a better comparison of the improved imaging and the implications for visual classification, please refer to Walmsley et al. (2021).

In this paper, we have a statistically robust sample size of both weak and strong bars, identified using Galaxy Zoo DECaLS (GZD). This sample was used to study the differences between weak and strong bars in the context of galaxy evolution, in particular the star formation rate, HI gas mass and depletion timescale. In addition, we aim to answer a more fundamental question: are weak and strong bars intrinsically different physical phenomena?

The structure of the paper is as follows. In Section 2 we describe Galaxy Zoo DECaLS in more detail, our data sources and the sample selection. The results are presented in Section 3 and discussed in Section 4. Finally, we end with our conclusions in Section 5. We assume a standard flat cosmological model using $H_0 = 70 \text{ km s}^{-1} \text{ Mpc}^{-1}$, $\Omega_m = 0.3$ and $\Omega_\Lambda = 0.7$ where necessary. Photometric quantities were taken from DECaLS (Dey et al. 2019).

2 DATA AND SAMPLE SELECTION

2.1 Galaxy Zoo, SDSS and DECaLS

The morphological classifications used in this paper were obtained from the Galaxy Zoo project, where citizen scientists classify galaxies according to a decision tree structure (Lintott et al. 2008, 2011). More specifically, we use the follow-up from Galaxy Zoo 2 (GZ2), namely Galaxy Zoo DECaLS (GZD, Walmsley et al. 2021). In GZ2, all images came from the Sloan Digital Sky Survey (SDSS, Gunn et al. 1998; York et al. 2000; Blanton et al. 2017) DR7 (Abazajian

et al. 2009), whereas GZD sourced their images from DECaLS (Dey et al. 2019). As DECaLS is a deeper survey (DECaLS has a median 5σ point source depth of $r = 23.6$, whereas SDSS DR7 is 95% complete to $r = 22.2$, Abazajian et al. 2009; Dey et al. 2019), this results in some previously invisible features now being visible. GZD only included galaxies that were also in SDSS DR11, which gives us the advantage that we can use preexisting SDSS data of these galaxies, including the Max Planck Institute for Astrophysics and the Johns Hopkins University (MPA-JHU) value added catalogue (VAC) (Kauffmann et al. 2003; Brinchmann et al. 2004; Tremonti et al. 2004). Nevertheless, this means that the magnitude limit of GZD equals the galaxy completeness limit of SDSS ($m_r = 17.77$, Strauss et al. 2002).

A second difference is that GZ2 only asked whether or not a certain galaxy had a bar, while GZD probes the strength of the bar as well by asking the volunteer whether the galaxy has a strong bar, a weak bar or no bar. A detailed explanation of GZD and its decision tree is provided by Walmsley et al. (2021).

Before moving on, we want to take some time explaining some common nomenclature unique to Galaxy Zoo that will be used frequently throughout this paper. The number of volunteers that answered a particular question, e.g., the bar question, is denoted as N_{bar} . The percentage of people that voted for a certain answer for a particular question, e.g., strong bar for the bar question, is denoted as $p_{\text{strong bar}}$ and is called the vote fraction. Finally, when considering the fraction of strong bars within a population, we denote it as $f_{\text{strong bar}}$ and call it the strong bar fraction.

2.2 ALFALFA and upper limits

This paper uses the Arecibo Legacy Fast ALFA (ALFALFA) catalogue of extragalactic HI sources (Giovannelli et al. 2005; Haynes et al. 2011, 2018) in order to assess HI gas masses. In ALFALFA, the HI gas mass is calculated using:

$$M_{\text{HI}} = 2.356 \times 10^5 D_{\text{Mpc}}^2 S_{\text{Jy km s}^{-1}}, \quad (1)$$

where S is the integrated HI line flux density in Jy km s^{-1} and D is the distance to the galaxy in Mpc. It is important to note that not all extragalactic sources are detected, as the chance of detection depends on both the integrated HI line flux and the width of the HI profile (Haynes et al. 2011, 2018). This problem is alleviated by estimating an upper limit for these non-detections. This can be done by rearranging Equation 4 of Haynes et al. (2018) to:

$$S_{\text{Jy km s}^{-1}} = \text{SNR} \times \text{RMS} \times W_{50} / \sqrt{W_{\text{smo}}}, \quad (2)$$

where W_{50} is the linewidth of the target (assumed to equal 200 km/s), w_{smo} is a smoothing width and equals $W_{50}/20$, RMS is the RMS noise and SNR is the signal-to-noise ratio. The SNR is assumed to equal 4.5, as the rate of detections in ALFALFA drops rapidly below $\text{SNR} = 4.5$. The RMS is extracted from the spectra, which have a spectral resolution of 10 km s^{-1} (Haynes et al. 2018), at the position of the non-detections. Finally, the HI gas mass upper limit can be computed by substituting the result of Equation 2 in Equation 1. We have assumed that all galaxies without gas measurements that are located within the ALFALFA footprint are non-detections. The footprint for the ALFALFA catalogue of extragalactic HI sources roughly corresponds to $07^{\text{h}}30^{\text{m}} < \text{R.A.} < 16^{\text{h}}30^{\text{m}}$ and $0^\circ < \text{Dec.} < +36^\circ$ for the northern hemisphere and $22^{\text{h}} < \text{R.A.} < 03^{\text{h}}$ and $0^\circ < \text{Dec.} < +36^\circ$

for the southern hemisphere (Haynes et al. 2018), although there is some fringing around the edges.

2.3 Sample selection

The whole of GZD has $\sim 314,000$ galaxies. However, this paper only uses the volunteer classifications from the latest GZD decision tree (GZD-5) and not the machine learning classifications from Walmsley et al. (2021). We also only considered galaxies with more than 30 total votes in order to exclusively work with galaxies with the most reliable classifications. This reduced the sample to 59,337 galaxies. In GZD, galaxies are classified according to a decision tree structure, which means that a volunteer will only answer “*Is there a bar feature through the centre of the galaxy?*” after they voted that the galaxy was a disk which is not viewed edge-on. The decision tree is shown (up to the bar question) in Figure 2.

We created a volume-limited sample from these 59,337 galaxies. The redshift range in our sample is $0.01 < z < 0.05$ in order to match the ALFALFA redshift range. To make this sample volume-limited, the dereddened DECaLS r -band absolute magnitude is constrained to $M_r < -18.96$. Additionally, our sample was also cross-matched against the MPA-JHU VAC (Kauffmann et al. 2003; Brinchmann et al. 2004; Tremonti et al. 2004) for stellar mass and (fibre) SFR measurements. This brought the number of galaxies down to 7,094.

As advised in Section 3.3 of Willett et al. (2013), we also apply limits on the percentage of people that voted that the galaxy has “features or a disk” ($p_{\text{features/disk}}$), the percentage of people that voted that the galaxy was not edge-on ($p_{\text{not edge-on}}$) and the amount of people that voted in the bar question (N_{bar}). Thresholds on these parameters are shown to limit our sample to not edge-on disk galaxies that may or may not contain bars. However, as the thresholds quoted in Willett et al. (2013) were calculated using the GZ2 dataset, we have to compute new values based on GZD using the method described in Willett et al. (2013). These new values are: $p_{\text{features/disk}} \geq 0.27$ and $p_{\text{not edge-on}} \geq 0.68$ for $N_{\text{bar}} \geq 20$, which brought the total number of galaxies with reliable classifications in our sample to 2,755. The effects of these cuts are shown in detail in Figure 2. Although we only require $p_{\text{features/disk}} \geq 0.27$, in practice, the value for $p_{\text{features/disk}}$ will be much higher. This is because most galaxies have a total of 40 unique classifications and we also limit our sample to galaxies that have $N_{\text{bar}} \geq 20$. For reference, the median $p_{\text{features/disk}}$ of our final sample is equal to 0.82 and the 10th percentile is still 0.58.

It is worth pointing out that the bar classifications might be affected by inclination. Even though we filter out the most edge-on galaxies, it is possible that the same bar in a face-on galaxy will be perceived differently by volunteers in a more inclined galaxy. Thus, a more stringent inclination threshold was considered. However, there is a trade-off between clean samples and sample size. We opted for a bigger sample size and judged that our threshold of $p_{\text{not edge-on}} \geq 0.68$ is sufficient for our purposes.

The last step in our sample selection is cross-matching against ALFALFA to obtain HI gas mass measurements (Giovannelli et al. 2005; Haynes et al. 2011, 2018), which reduced the final sample size to 1,867 galaxies.

Every galaxy was assigned one of three bar types (strong, weak or no bar) using the following scheme: if $p_{\text{strong bar}} + p_{\text{weak bar}} < 0.5$, the galaxy had no bar. If the previous condition was not met and if $p_{\text{strong bar}} \geq p_{\text{weak bar}}$, then the galaxy had a strong bar. If not, it had a weak bar. This scheme is summarized in Table 1. This resulted in 15.5% of our galaxies (289/1,867) having a strong bar, 28.1%

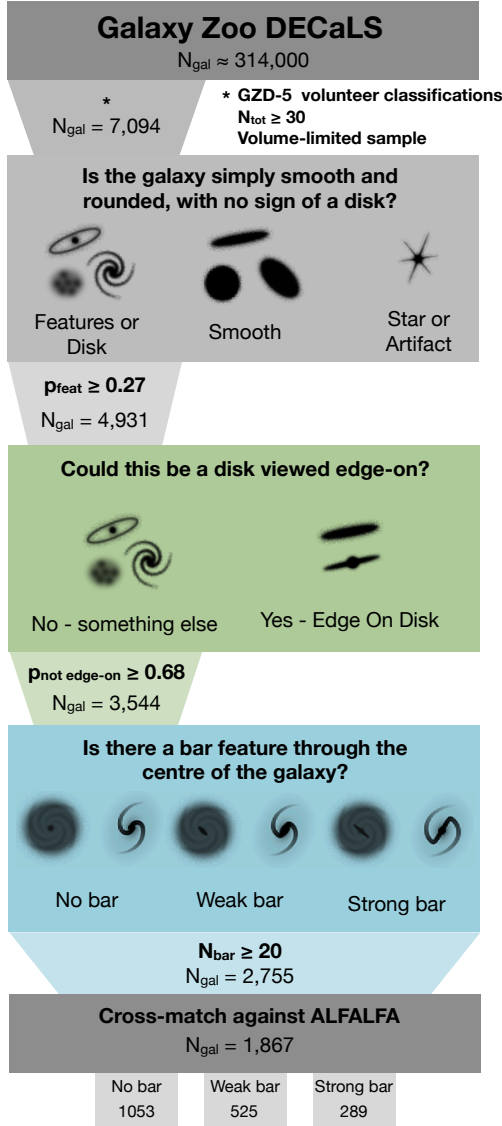


Figure 2. Visualisation of the decision tree structure of GZD, up to the bar question. Note that users will only reach the bar question if they said the galaxy was a disk galaxy that is not viewed edge-on. The thresholds and their effect on the amount of galaxies in our sample are visualised in the funnels between each step. The thresholds on $p_{\text{features/disk}}$, $p_{\text{not edge-on}}$ and N_{bar} are calculated using the method described in Willett et al. (2013). Please refer to Walmsley et al. (2021) for the complete decision tree.

Table 1. Every galaxy is assigned a bar type (strong bar, weak bar and no bar) based on their respective vote fractions ($p_{\text{strong bar}}$, $p_{\text{weak bar}}$ and $p_{\text{no bar}}$) according to the following scheme.

Condition 1	Condition 2	Result
$p_{\text{strong bar}} + p_{\text{weak bar}} < 0.5$	N/A	No bar
$p_{\text{strong bar}} + p_{\text{weak bar}} \geq 0.5$	$p_{\text{strong bar}} < p_{\text{weak bar}}$	Weak bar
$p_{\text{strong bar}} + p_{\text{weak bar}} \geq 0.5$	$p_{\text{strong bar}} \geq p_{\text{weak bar}}$	Strong bar

(525/1,867) having a weak bar and 56.4% (1,053/1,867) having no bar. Thus, the total barred fraction equals 43.6%, in general agreement with the literature (de Vaucouleurs et al. 1991; Eskridge et al. 2000; Men endez-Delmestre et al. 2007; Barazza et al. 2008; Aguerri et al. 2009; Nair & Abraham 2010a; Masters et al. 2011; Buta et al. 2019; Zhao et al. 2020), although we study and compare bar fractions in more detail in Sections 2.5.1 and 3.1. Figure 3 shows random examples of galaxies with a strong or a weak bar.

2.4 Bar length measurements

In an analysis of bar types, bar length measurements are desirable. A citizen science project aimed at measuring bar lengths for GZ2 galaxies was previously carried out by Hoyle et al. (2011)¹. However, only ~22% of the galaxies in our volume-limited sample had bar length measurements in Hoyle et al. (2011). To alleviate this issue, one of the authors (TG) measured the bar length of all galaxies with a weak or strong bar in our volume-limited sample of GZD (a total of 814 bars). Of those, 177 also appeared in Hoyle et al. (2011). An additional 60 galaxies from Hoyle et al. (2011) (that were not in GZD) were measured as well to better compare the two bar length catalogues. This brought the total amount of bar length measurements to 874. Here, bar length is defined as the length of the entire bar (i.e., twice the bar radius). Every galaxy was measured twice and the average length (in arcsec) was taken. The order of the measurements was randomized, so that it was unknown while measuring whether the bar was classified by GZD as weak or strong. We used the angular diameter distance (which was calculated using SDSS redshifts) to convert these bar lengths from arcsec into kpc.

Our bar length measurements and those of Hoyle et al. (2011) agree fairly well (Figure 4). On average, our bar length measurements are 87.8% the size of those in Hoyle et al. (2011). This difference is likely to result from us having access to deeper and more detailed DECaLS images with a smaller PSF, whereas Hoyle et al. (2011) used SDSS DR6 (Adelman-McCarthy et al. 2008) images on a Google Maps interface.

We also compute the relative bar length, obtained by dividing the length of the bar by the diameter of the galaxy. We opted to use the well-established Petrosian radii from SDSS-IV DR16 to calculate the Petrosian diameter (Blanton et al. 2017; Ahumada et al. 2020).

2.5 Comparison to other catalogues

2.5.1 Galaxy Zoo 2

It is important to verify whether different versions of Galaxy Zoo are consistent with each other. Therefore, we compare the results of GZD with GZ2. In order to do this, we cross-matched our sample with GZ2, using the appropriate cuts for GZ2 (see Willett et al. 2013). A total of 1,160 galaxies overlap in both samples. Note that, as we are using raw vote fractions in GZD, we are comparing them to the raw vote fractions of GZ2 in order to compare like with like. For more information on GZ2 raw and debiased vote fractions, please refer to Willett et al. (2013) and Hart et al. (2016) and to Walmsley et al. (2021) for a broader comparison of GZ2 with GZD.

¹ The bar length values in Hoyle et al. (2011) are quoted in units of kpc/h. However, closer inspection revealed that this is an error, and the bar lengths given by Hoyle et al. (2011) are actually in kpc. We have made this correction throughout this work.

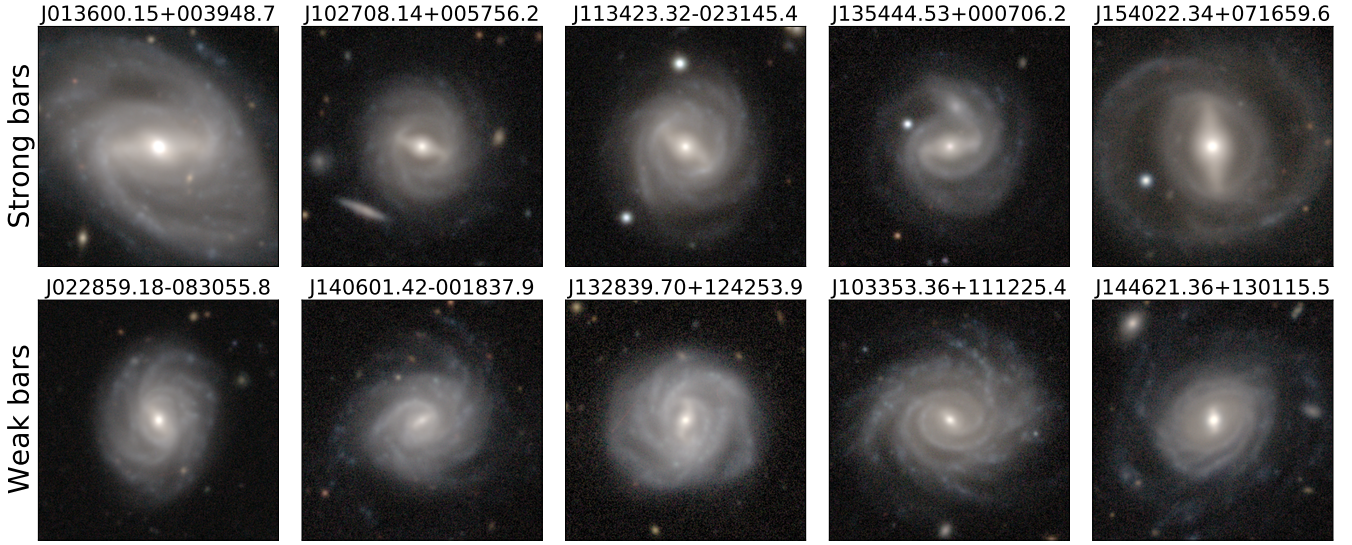


Figure 3. DECaLS postage stamps (72x72 arcsec) of five randomly selected galaxies with high Petrosian radii (> 18 arcsec) and high strong bar vote fractions ($p_{\text{strong bar}} > 0.6$, top row) and weak bar vote fractions ($p_{\text{weak bar}} > 0.6$, bottom row) in GZD. Notice the difference in bar length and strength between the strong and weak bars.

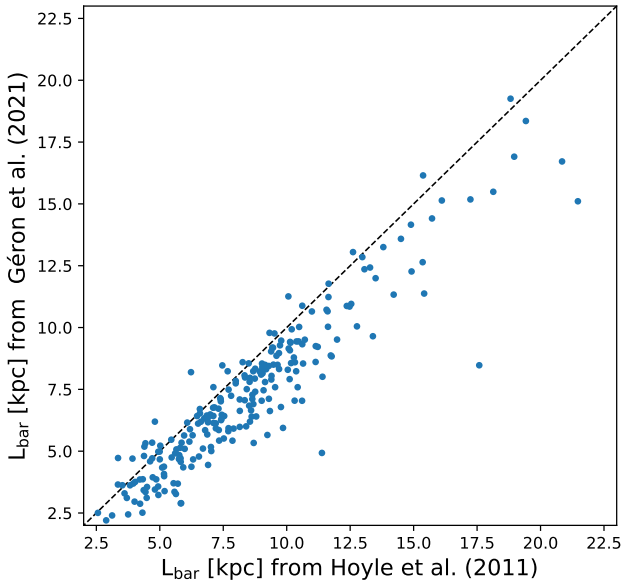


Figure 4. A comparison between the bar lengths measured in this study and those of Hoyle et al. (2011) for 237 cross-matched galaxies. The dashed line indicates where the measurements would be identical. Our measurements are, on average, 87.8% the size of those of Hoyle et al. (2011). This difference is the result of different imaging used: Hoyle et al. (2011) used SDSS DR6, while we had access to deeper DECaLS images. See Section 2.4 for details on how these bar lengths were measured.

In the left panel of Figure 5, the GZ2 bar fraction, as well as the GZD weak bar fraction, the GZD strong bar fraction and the GZD total bar fraction are visualised over redshift. GZ2 bars were identified by using a $p_{\text{bar, GZ2}}$ threshold of 0.5, similarly to many previous GZ2 studies (Masters et al. 2011, 2012; Cheung et al. 2015; Kruk et al. 2017, 2018). The GZD bars were identified according to the scheme described in Table 1. We can very clearly

see that we identify many more bars with GZD. In fact, we find as many weak bars in GZD as there were bars in GZ2. This can be due to either deeper imaging (provided by DECaLS) or due to the different decision trees employed. It is possible that in GZ2, because volunteers were not given an intermediate option, they defaulted to a ‘no bar’ classification when unsure.

If the latter effect plays a significant role in our increased observed bar fraction, then many of our GZD galaxies with a weak bar will have low to average GZ2 bar vote fractions ($p_{\text{bar, GZ2}}$). This is indeed what we observe in the right panel of Figure 5. Here, the raw GZ2 vote fraction is plotted against the GZD bar fraction. As an illustration, the galaxies with a GZ2 vote fraction of ~ 0.4 have an average GZD weak barred fraction of ~ 0.6 . As noted before, many previous GZ2 studies used $p_{\text{bar, GZ2}} = 0.5$ as a threshold to select bars (Masters et al. 2011, 2012; Cheung et al. 2013, 2015; Kruk et al. 2017, 2018). Here, we see that the strong bar fraction is very low in the $p_{\text{bar, GZ2}} < 0.5$ range, suggesting that the vast majority of the GZD galaxies with a strong bar were already picked up by GZ2, while most newly found barred galaxies in GZD have a weak bar. Previous GZ2 studies usually noted that their barred sample mainly consisted of strongly barred galaxies (Masters et al. 2011; Cheung et al. 2013, 2015; Kruk et al. 2017, 2018). For example, Masters et al. (2012) found that $>90\%$ of the strong and intermediate bar types from Nair & Abraham (2010a) have $p_{\text{bar, GZ2}} > 0.5$. This notion is now verified by GZD as well and suggests that results from previous GZ2 studies mainly apply to strongly barred galaxies, not weakly barred galaxies.

The weak bar fraction rises from ~ 0.0 up to ~ 0.7 in the $p_{\text{bar, GZ2}} < 0.5$ range. In addition, the GZD weak bar fraction is still quite high in the $p_{\text{bar, GZ2}} > 0.5$ range (at a GZ2 vote fraction of ~ 0.8 , the GZD weak bar fraction is still ~ 0.4). These galaxies are thought to have a very clear weak bar, which is not necessarily the same as having a strong bar. Examples of very clear weak bars are shown in the bottom row of Figure 3. Finally, the GZD strong bar fraction and GZD total bar fraction correlate nicely with the GZ2 vote fraction.

In conclusion, the GZD total barred vote fraction is higher than

Table 2. A comparison between GZD and the catalogue of visual morphological classifications of [Nair & Abraham \(2010a\)](#). **Top row:** GZD galaxies with a strong bar. **Middle row:** GZD galaxies with a weak bar. **Bottom row:** GZD galaxies without bars. Each cell indicates the percent of GZD bars that are classified by [Nair & Abraham \(2010a\)](#) as having a given feature, with the sample size in parentheses. E.g.: 21.4% of the GZD galaxies with a strong bar are also classified as strongly barred by [Nair & Abraham \(2010a\)](#).

NA10 GZD	Strong bar	Intermediate bar	Weak bar	No bar	Others
Strong bar	21.4% (25)	43.6% (51)	8.5% (10)	19.7% (23)	6.8% (8)
Weak bar	1.3% (2)	27.1% (42)	23.9% (37)	42.6% (66)	5.2% (8)
No bar	0.0% (0)	1.2% (4)	5.3% (18)	90.5% (306)	3.0% (10)

the GZ2 barred vote fraction due to deeper imaging and an improved decision tree. The GZD strong bar fraction correlates with the GZ2 barred vote fraction. Most GZD strong bars were already identified in GZ2, while weak bars make up the bulk of the newly detected bars in GZD, compared with GZ2.

2.5.2 *Nair and Abraham*

A comparison of our GZD sample with the catalogue of visual morphological classifications of [Nair & Abraham \(2010a\)](#) is shown in Table 2. A total of 589 galaxies appear in both samples. GZD classifies galaxies into having no bar, a weak bar or a strong bar, whereas [Nair & Abraham \(2010a\)](#) has many more options: strong, intermediate, weak, ansae, peanut, nuclear, unsure or no bar. However, the ansae, peanut, nuclear and unsure categories are rare and were combined into one category called ‘others’ in our comparison. It is also worth noting that a single galaxy can have multiple classifications in [Nair & Abraham \(2010a\)](#), but this did not occur frequently.

A total of 25 out of 27 galaxies classified by [Nair & Abraham \(2010a\)](#) as being strongly barred are also identified in GZD as having a strong bar. Also, 306 out of 338 of the galaxies we classified as having no bar were also classified by [Nair & Abraham \(2010a\)](#) as being unbarred. Not a single galaxy we classified as having no bar was classified as strongly barred by [Nair & Abraham \(2010a\)](#). However, there is a small subset of galaxies (23 in total) that volunteers classified as having a strong bar in GZD, while they were identified as being unbarred in [Nair & Abraham \(2010a\)](#). The authors of this paper visually inspected those galaxies separately and concluded that the most of them do have a strong bar (see Appendix A). A possibility for this apparent contradiction is that [Nair & Abraham \(2010a\)](#) classified galaxies based on SDSS images, while the volunteers got shown deeper and more detailed DECaLS images.

3 RESULTS

3.1 Demographics of galaxies hosting bars

3.1.1 *Properties of galaxies hosting weak and strong bars*

Previous studies have found that bars are more likely to be found in massive, red, quiescent galaxies ([Masters et al. 2012](#); [Cervantes Sodi 2017](#)), but they did not distinguish between weak and strong bars. In Figure 6, we show how the GZD galaxy population with a weak or strong bar changes in terms of (g-r) colour, stellar mass, global SFR and fibre SFR. The latter three parameters were taken from the MPA-JHU catalogue ([Kauffmann et al. 2003](#); [Brinchmann et al. 2004](#); [Tremonti et al. 2004](#)). The reason we included fibre SFR in this analysis is because this probes the SFR in the central 3 arcsecs of the galaxy. As bars are thought to funnel gas to the centre

and increase SFR there, this region is of most interest to determine the effect of the bar. However, the physical size that the 3 arcsec region of the fibre probes will change depending on the redshift of the galaxy. For our sample, it varies between 0.69 and 2.93 kpc. However, as we expect no changes in the proportion of bar types over the small redshift range we are probing, this effect is negligible as it will affect the three groups equally. For more details, please refer to Appendix B.

The distribution of the bar types for every parameter in Figure 6 is shown in terms of bar fractions (the lines, secondary y-axis) and counts (histograms, normalised so that the area under each histogram equals one, primary y-axis). The top-left plot of Figure 6 shows the (g-r) colour. We see that the strong bar fraction increases at redder colours, in agreement with the literature ([Masters et al. 2012](#); [Cervantes Sodi 2017](#)). There are few strong bars in the blue region. In contrast, the weak bar fraction decreases with redder colours. It is interesting to note the similarity between the shapes of the ‘combined’ fraction and Figure 3 in [Masters et al. \(2011\)](#), a previous GZ study looking at bar fraction against (g-r) colour, especially at redder colours.

The top right plot shows the stellar mass distribution of the different bar types. Again, we see that the strong bar fraction rises with stellar mass. However, this is again not the case for weak bars. Notice the high weak bar fraction for low-mass ($M_* < 10^{10} M_\odot$) galaxies. [Elmegreen & Elmegreen \(1985\)](#) also found more weak bars among low-mass galaxies.

The bottom left panel displays the total SFR. The ‘combined’ bar fraction decreases slightly with total SFR. It is also worth noting the difference between the bar fraction and the histogram. Whereas the strong bar fraction is highest at the lowest total SFRs, it seems that most strong bars (similar to most of the galaxies in our sample) are actually situated in the middle total SFR range ($\text{SFR} \sim 1 M_\odot \text{yr}^{-1}$).

When looking at the fibre SFRs (bottom right), we see that the strong bar fraction is highest at the lowest and highest fibre SFRs. The ‘combined’ and weak bar fractions display more complicated behaviour with no clear trend.

In conclusion, the general consensus that bars appear more often in massive, red and quiescent galaxies seems to hold true, but only for strong bars. The fraction of weak bars, in contrast, is higher among low-mass and blue galaxies than in massive and red galaxies.

3.1.2 *Colour-magnitude diagram and SFR-mass plane*

To expand on the idea that strong bars are preferentially found in massive, red, quiescent galaxies, we study the location of each type of bar on the colour-magnitude plane and SFR-mass plane. The colour-magnitude plane is shown in Figure 7. We used the ‘blue edge of the red sequence’ defined in [Masters et al. \(2010\)](#) to divide our sample into red sequence and blue cloud galaxies.

The weak bar fraction is slightly higher in blue cloud galaxies than in red sequence galaxies, but not by much (29.9% and 25.2%, respectively). The strong bar fraction is clearly higher in the red sequence (24.9%) than in the blue cloud (9.6%). A KS test reveals that the colour distribution of galaxies with strong bars is very significantly different from the unbarred colour distribution (p-value $< 10^{-15}$), suggesting that a strong bar influences the colour of its host galaxy and possibly, its evolution. The colour distribution of galaxies with weak bars compared to that of unbarred galaxies is less significantly different (p-value = 0.012), but still remarkable.

Interestingly, the absolute magnitude distributions of galaxies

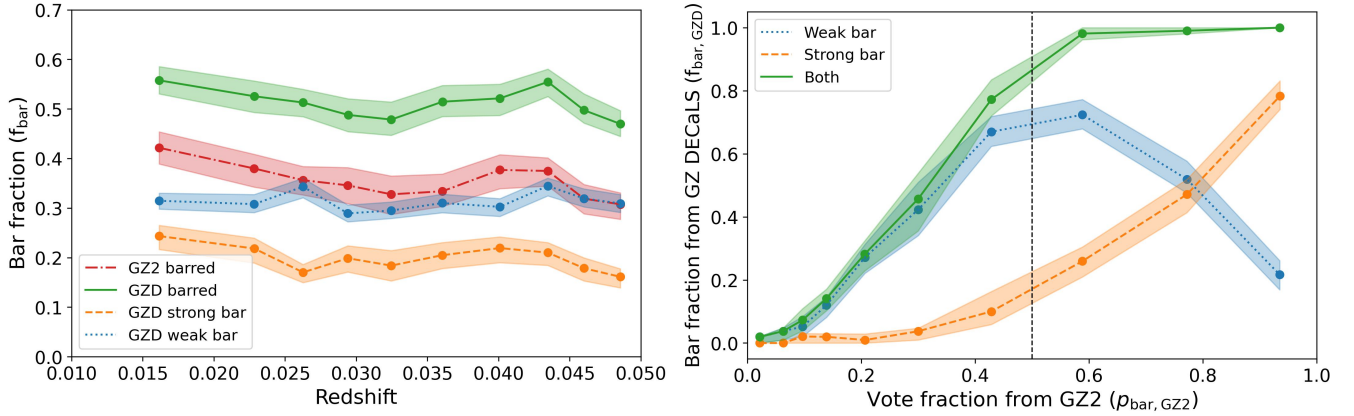


Figure 5. A comparison between Galaxy Zoo 2 (Willett et al. 2013) and GZD. **Left:** The various bar fractions (from GZD and GZ2) over redshift for the galaxies in that are in both catalogues. All the galaxies are binned in equal-sized bins. **Right:** The various GZD bar fractions ($f_{\text{bar, GZD}}$) compared to the GZ2 vote fraction ($p_{\text{bar, GZ2}}$). The contours represent the 3σ region after bootstrapping the data 10,000 times and retaining 90% of the data for each iteration. The vertical dashed line represents the threshold many GZ2 studies use to select bars ($p_{\text{bar, GZ2}} > 0.5$). It is clear that GZD identifies many more barred structures than GZ2. Most of the ‘newly barred’ galaxies in GZD appear have a weak bar.

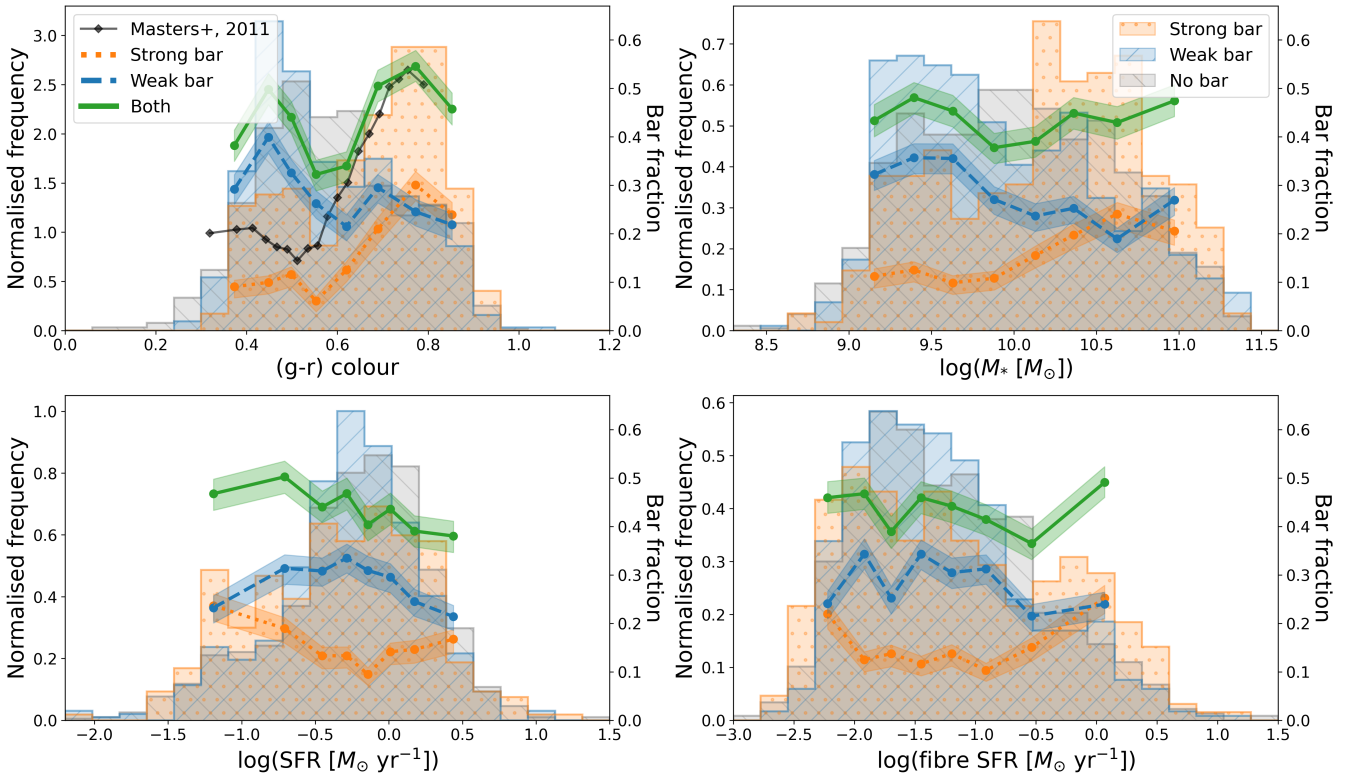


Figure 6. **Top left:** The effect of (g-r) colour on weak, strong and combined bar fraction (secondary y-axis). All the galaxies are binned in equal-sized bins. The contours represent the 3σ region after bootstrapping the data 10,000 times and retaining 90% of the data for each iteration. The histograms in the background show the normalised frequencies of galaxies with a strong bar, a weak bar and no bar (primary y-axis). **Top right:** The effect of stellar mass on the various bar fractions. **Bottom left:** The effect of SFR. **Bottom right:** The effect of fibre SFR. This figure shows that strong bars drive the consensus that bars appear more often massive, red and quiescent galaxies. The weak bar fraction actually decreases with colour and stellar mass. Magnitudes obtained from SDSS and SFRs, fibre SFRs and stellar masses obtained from MPA-JHU.

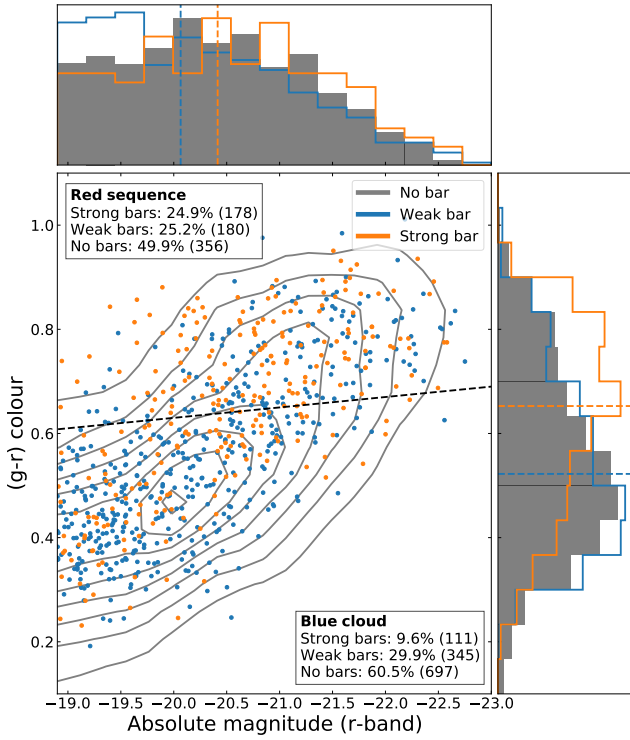


Figure 7. Location of all galaxies with a strong bar (orange) and a weak bar (blue) on the colour-magnitude diagram. The contour plot in the background shows the location of all the galaxies without bars. The dashed line across the plane defines the “blue edge of the red sequence” and effectively divides the sample into the blue cloud (underneath the line) and the red sequence (above the line, defined in [Masters et al. 2010](#)). The histograms on top and on the right side of the main panel are normalised histograms of the absolute r-band magnitude and (g-r) color, respectively, for our three different groups. The galaxies with a weak bar seem to be distributed equally across the plane, while the galaxies with a strong bar are clustered around the red sequence.

with a weak bar and no bar are significantly different (p-value = 0.009), which suggests a significant population of low-mass galaxies with a weak bar, similar to what we saw in Section 3.1.1. This difference is not observed for between galaxies with a strong bar and no bar (p-value = 0.98).

We can also plot our galaxies on a SFR - stellar mass plane, shown in Figure 8. On this plane, galaxies tend to cluster naturally into a star forming (SF) group and a quiescent group. Those groups are separated here by using the star formation sequence (SFS) defined by [Belfiore et al. \(2018\)](#):

$$\log \left(\text{SFR} / M_{\odot} \text{ yr}^{-1} \right) = (0.73 \pm 0.03) \log (M_{*} / M_{\odot}) - (7.33 \pm 0.29), \quad (3)$$

and assuming anything that is 1σ ($= 0.39$ dex) below this line is quiescent and everything else star forming (visualised in Figure 8 by the dashed line).

Again, the weak bar fractions are similar in the quiescent group and the SF group (25.0% and 29.3%, respectively) whereas the strong bar fraction is higher in the quiescent group than in the SF group (22.0% and 13.0%, respectively). However, it is interesting to note that in absolute numbers, there are actually more SF strong bars (176) than quiescent strong bars (113). Also, we can clearly see

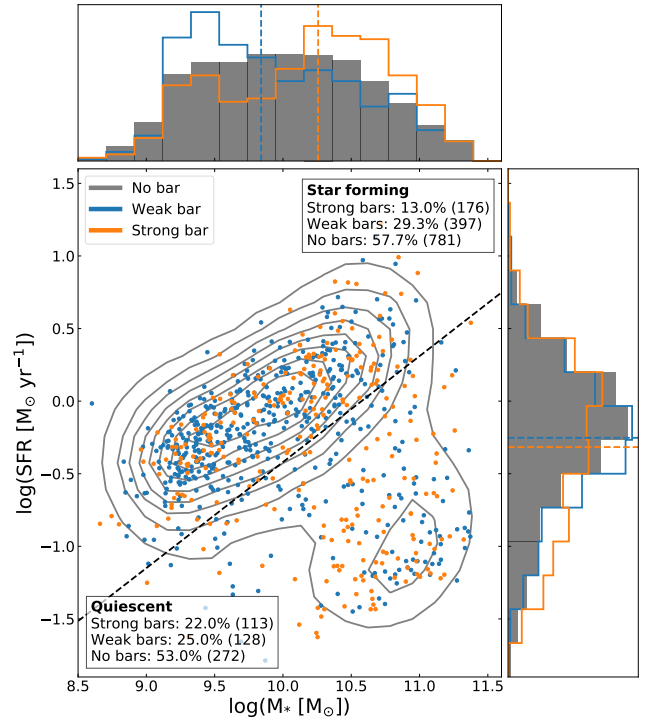


Figure 8. Location of all galaxies with a strong bar (orange) and a weak bar (blue) on the SFR - stellar mass plane. The contour plot in the background shows the location of all the galaxies without bars. The dashed line across the plane divides the sample into a SF region (above the line) and a quiescent region (under the line, defined in [Belfiore et al. 2018](#)). The histograms on top and on the right side of the main panel are normalised histograms of the stellar mass and SFR, respectively, for our three different groups. The strong bar fraction is higher in the quiescent region than in the SF region, whereas the weak bar fraction is similar in both regions.

the difference in the stellar mass distributions between galaxies with a weak bar and unbarred galaxies, (p-value = 0.001). This confirms what we observed above; that there is a significant population of low-mass galaxies with a weak bar. In contrast, there seem to be more high-mass galaxies with a strong bar than unbarred galaxies (p-value $< 10^{-6}$).

These results agree with our previous statement: that galaxies with a strong bar drive the observation that bars appear more often in massive, red quiescent galaxies. Weak bars appear in similar fractions in SF and quiescent groups. However, as noted by previous studies ([Masters et al. 2012](#)), this can be interpreted in various ways: is it the strong bars that cause the transition from the SF group to the quiescent group by quenching the galaxy or is it easier to form strong bars in quenched galaxies? We discuss this further in Section 3.3.

3.2 Bar length

From a quick glance at Figure 3, we can already see that strong bars tend to be longer than weak bars. This is very unsurprising, as we tell the volunteers that strong bars “*extend across a large fraction of the galaxy*” while weak bars are “*smaller and fainter relative to the galaxy*”. This is quantitatively verified in Figure 9, where we show the distribution of bar lengths of our sample (see Section 2.4 for details on how the bar length was measured). We split up the

sample, not only in weak and strong, but also into quiescent and SF, according to the cutoff described in Section 3.1.2, so we have a total of 4 subsamples. The bar length is shown in kpc in the left panel. Interestingly, we observe that SF and quiescent bars of the same bar type are not the same length. Bars in quiescent galaxies are, on average, longer than the bars in SF galaxies, for both weak and strong bars. Also, the average quiescent weak bar is about as long as the average SF strong bar. The shortest bars are typically weak bars in SF galaxies, while the longest bars are typically strong bars in quiescent galaxies.

To estimate the length of the bar in relation to its host, we also calculated the relative bar length (right panel of Figure 9), obtained by dividing the absolute bar length by the SDSS r-band Petrosian diameter (the Petrosian radius times two). We find that bars in SF and quiescent galaxies with the same bar type have roughly the same relative length. Strong bars are on average longer than weak bars in terms of relative bar length. A weak bar will, on average, cover 20-30% of the Petrosian diameter, whereas a strong bar will span over, on average, 40-45% of the Petrosian diameter.

Again, it is worth stressing that we expected strong bars to be longer than weak bars, as this is what we asked the volunteers to select for. However, it is interesting to note that there is still quite an overlap in (absolute and relative) bar length between weak and strong bars.

Interestingly, we see that strong bars in quiescent galaxies are longer (in terms of absolute bar length) than strong bars in SF galaxies. A possibility is that bars are still growing (and possibly helping to quench their host) when in SF galaxies and are fully grown once their host becomes quiescent. Additionally, the relative bar size of strong bars in quiescent and SF galaxies is similar, which suggests that the bar co-evolves with the entire galaxy and showcases that bars have an important role in galaxy evolution. Similar results are observed for weak bars.

However, the plot on the left side of Figure 9 can be a natural consequence of the volunteers classifying bars into weak and strong based on the relative bar length and the fact that quiescent galaxies tend to be larger than SF galaxies. Please refer to Appendix C for a more detailed discussion on this topic.

3.3 Addressing causality

We have found that the fraction of galaxies with a strong bar is notably higher in quiescent galaxies than in SF galaxies, whereas this was not found for weak galaxies. However, it is not clear whether strong bars help to quench their host or whether it is easier to form strong bars in quenched galaxies.

In an attempt to address this problem of causality, we look more closely at the SFR in the central 3 arcsec of the galaxy - the fibre SFR - as that is where we expect to see a difference in SFR caused by the bar if bars drive gas to the centre. Additionally, the global SFRs estimates from Brinchmann et al. (2004) are in part based on the colour outside the fibre. However, we know from Kruk et al. (2018) that bars are redder than discs. Given that we are comparing different bar types, we are unsure if this will affect our bar types differently and therefore decided to work solely with SFR estimates based on emission lines in the fibre instead.

As the Kennicutt-Schmidt law (Kennicutt 1998a,b) implies a relation between SFR and gas, we are also interested in potential differences in gas mass as well. For this, we use the gas mass measurements from the ALFALFA catalog of extragalactic HI sources (Giovanelli et al. 2005; Haynes et al. 2011, 2018). In order to accommodate for the non-detections in ALFALFA (see Section 2.2),

we perform a survival analysis on the data using the Python package ‘lifelines’ (Davidson-Pilon et al. 2020)². Survival analysis is a statistical technique that allows us to compare two populations that have left-censored data points in a certain parameter (in our case: ALFALFA upper limits for gas mass) by correctly constructing the cumulative density function (CDF) for that parameter. We use the well established Cox’s proportional hazards model (Cox 1972) to quantify the effect of every bar type on the CDF. It is a type of regression that allows for censored data and is often used in conjunction with survival analysis. Finally, we also divide our sample in a quiescent and SF group, as shown in Figure 8, to compare like with like: SF strong bars with SF weak bars and quiescent strong bars with quiescent weak bars.

The results are shown in Figure 10. The top row displays the results for HI gas mass. It seems that SF galaxies with a strong bar or a weak bar have significantly less HI gas than SF unbarred galaxies, with galaxies with a strong bar having the lowest amount of HI gas. The CDFs of the fibre SFRs are shown in the middle row of Figure 10. The SF galaxies with a strong bar have significantly higher values for fibre SFR than both SF galaxies with a weak bar or no bar. There are no significant differences between SF galaxies with a weak bar and unbarred galaxies in terms of fibre SFR. No significant differences were observed among quiescent galaxies.

We can put a timescale on these effects by combining the two parameters above (fibre SFR and HI gas mass) into the depletion timescale:

$$\tau_{\text{dep}} = \frac{M_{\text{gas}}}{\text{fibre SFR}}, \quad (4)$$

which probes how quickly a galaxy will consume its gas reservoir for a given SFR (Janowiecki et al. 2020). Galaxies with a long depletion timescale will take a long time before they run through their gas reservoir, and the opposite is true for galaxies with short depletion timescales (assuming all the gas in the reservoir will be available for star formation). The depletion timescale might be a too simplistic metric, as Janowiecki et al. (2020) noted that it assumes a constant SFR and that gas recycling is non-existent, while other work (Kannappan et al. 2013) has shown that refueling on ~Gyr timescales can happen in SF galaxies. Also, we use fibre SFR to calculate the depletion timescale, while others use the global SFR. Thus, the depletion timescales shown here are in fact depletion timescales for the centre of the galaxy (or we have to assume little to no SF outside the fibre, which is unlikely). Additionally, we have to point out that, while the fibre SFR only probes the centre, the gas mass estimates are global gas masses. Finally, we are also using HI gas measurements rather than molecular gas. All this results in the relatively high values for the depletion timescale. However, these issues affect all galaxies in our sample in the same way, so it is still a useful metric.

The depletion timescale is shown in the bottom row of Figure 10. We see that the SF galaxies with a strong bar have a significantly shorter depletion timescale than the SF galaxies with a weak bar or no bar. This result implies that SF galaxies with a strong bar are rapidly evolving and use up their gas quicker due to increased central SFRs. However, it is important to note that this was only seen in SF galaxies. The various bar types show almost no significant differences when their host is quiescent.

However, stellar mass also correlates with both gas mass and (fibre) SFR (Brinchmann & Ellis 2000; Brinchmann et al. 2004;

² lifelines: <https://lifelines.readthedocs.io/en/latest/#>

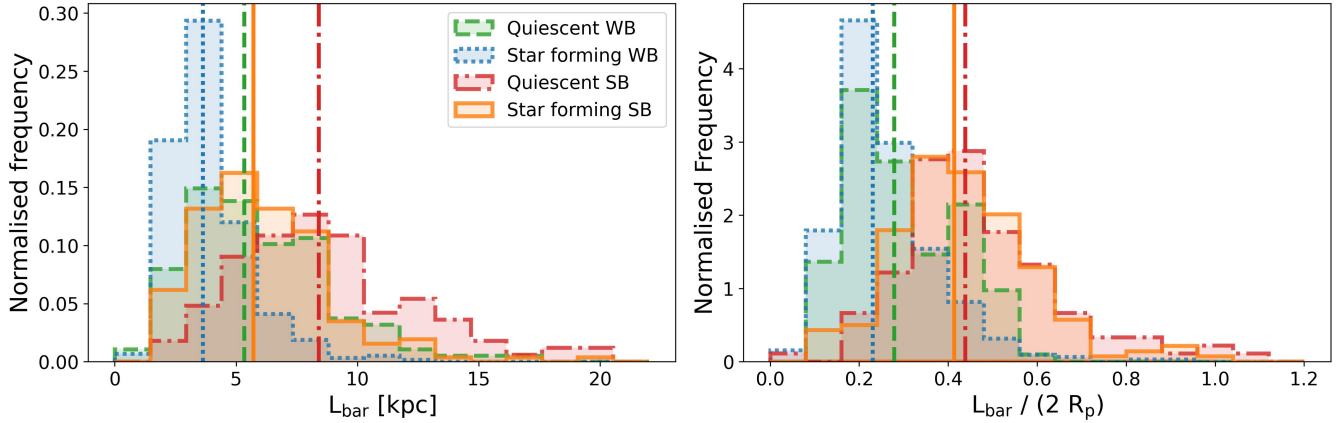


Figure 9. **Left:** The distribution of bar lengths for the different bar types in absolute units (kpc). **Right:** The distribution of bar lengths in relative units, obtained by dividing the absolute bar length by the SDSS r-band Petrosian diameter (or twice the Petrosian radius, R_p). In terms of absolute bar length, quiescent galaxies with a weak (strong) bar are longer than SF galaxies with a weak (strong) bar. When looking at relative bar length, quiescent and SF galaxies of the same bar type have similar bar lengths. A strong bar will span, on average, 40–45% of the Petrosian diameter of its host, while a weak bar will cover 20–30%.

Noeske et al. 2007; Lara-López et al. 2010). In addition, as we have noted above, there are differences in the stellar mass distribution between galaxies with a weak and strong bar.

This bias is filtered out by plotting the parameters above against stellar mass and assessing their relation with the Python package ‘linmix’³, which is based on the hierarchical Bayesian model of Kelly (2007). This technique allows us to fit a linear relationship to data with two-dimensional uncertainties as well as correctly taking into account the censored data from ALFALFA. It works by running a Markov chain Monte Carlo (MCMC) algorithm to sample the posterior distribution, given the data, which one can use to correctly estimate the errors on the fit. As we only observe significant differences between the bar types in the SF galaxies in Figure 10, we only look at the SF galaxies here.

The one-dimensional relations created with linmix are visualised in Figure 11. The top row shows HI gas mass for unbarred galaxies (left column, black), galaxies with a weak bar (middle column, blue) and galaxies with a strong bar (right column, orange). The contours show the 2σ uncertainty on the fit. To facilitate comparison, the trend for the unbarred galaxies is displayed with a dashed line in all subplots. We see that galaxies with a strong bar have lower HI gas masses, except at the lowest stellar mass range ($10^{9.5} M_\odot < M_*$) compared to unbarred galaxies. The trend for galaxies with a weak bar is also lower and less steep than the trend for unbarred galaxies, but the 2σ uncertainty contours partially overlap, suggesting that this isn’t as significantly different.

The middle row of Figure 11 displays the trends for fibre SFR. Galaxies with a weak bar and unbarred galaxies do not have significantly different trends. However, the trend of galaxies with a strong bar is steeper than that of the unbarred galaxies, which shows that SF galaxies with a strong bar have higher fibre SFRs, especially at higher stellar masses. The depletion timescale trends show a similar result: galaxies with a weak bar and unbarred galaxies do not differ much, while galaxies with a strong bar have shorter depletion timescales, especially at higher stellar masses.

We have also made Figures 10 and 11 for our sample with a more stringent inclination cut of $i < 45^\circ$ (not shown). The in-

clination measurements used were calculated using the adaptive moments from SDSS DR16 (Ahumada et al. 2020). We saw that the difference between strong and weak bars became more prominent and more statistically different for fibre SFR and depletion timescale. This is most likely because a stricter inclination threshold results in cleaner samples (at the cost of a lower sample size). However, the opposite was true for HI gas mass, whose trends became more uncertain and less statistically different. We assume this is due to the extra uncertainties associated with the non-detections in ALFALFA and the resultant few actual detections when limiting our sample to $i < 45^\circ$. To avoid this low sample size, we decided to not apply this additional inclination threshold throughout the paper and used our current threshold based on $p_{\text{not edge-on}}$ instead.

The two different methods applied to our sample show the same result: that SF galaxies with a strong bar differ significantly from SF galaxies with a weak bar and unbarred galaxies, who do not differ from each other as much. SF galaxies with a strong bar have lower HI gas mass, possibly due to higher fibre SFRs, which results in shorter depletion timescales. This implies that SF galaxies with a strong bar are rapidly evolving galaxies, which quench faster than their weakly barred and unbarred counterparts.

3.4 Are weak and strong bars distinct populations?

We have shown that, on average, SF galaxies with a strong bar have higher fibre SFRs than SF galaxies with a weak bar at a given stellar mass. The next question to ask is: is there a measurable difference between strong and weak bars when controlling for bar length? In Figure 12, we plot fibre SFR against the length of the bar for four different subgroups: SF galaxies with a strong bar, SF galaxies with a weak bar, quiescent galaxies with a strong bar and quiescent galaxies with a weak bar. The length of the bar is measured in absolute units (left panel) and relative units, obtained by dividing the absolute length by the Petrosian diameter (right panel). Interestingly, with both measures of bar length, we see that galaxies with a strong bar do not have higher fibre SFR than galaxies with a weak bar for a given bar length. This suggests that both strong and weak bars have similar influences on their host galaxy (i.e., funnel gas to the centre, where it is used to increase SFR) when controlling for bar length. However, for SF galaxies in general, we do see that fibre

³ linmix: <http://linmix.readthedocs.org/>

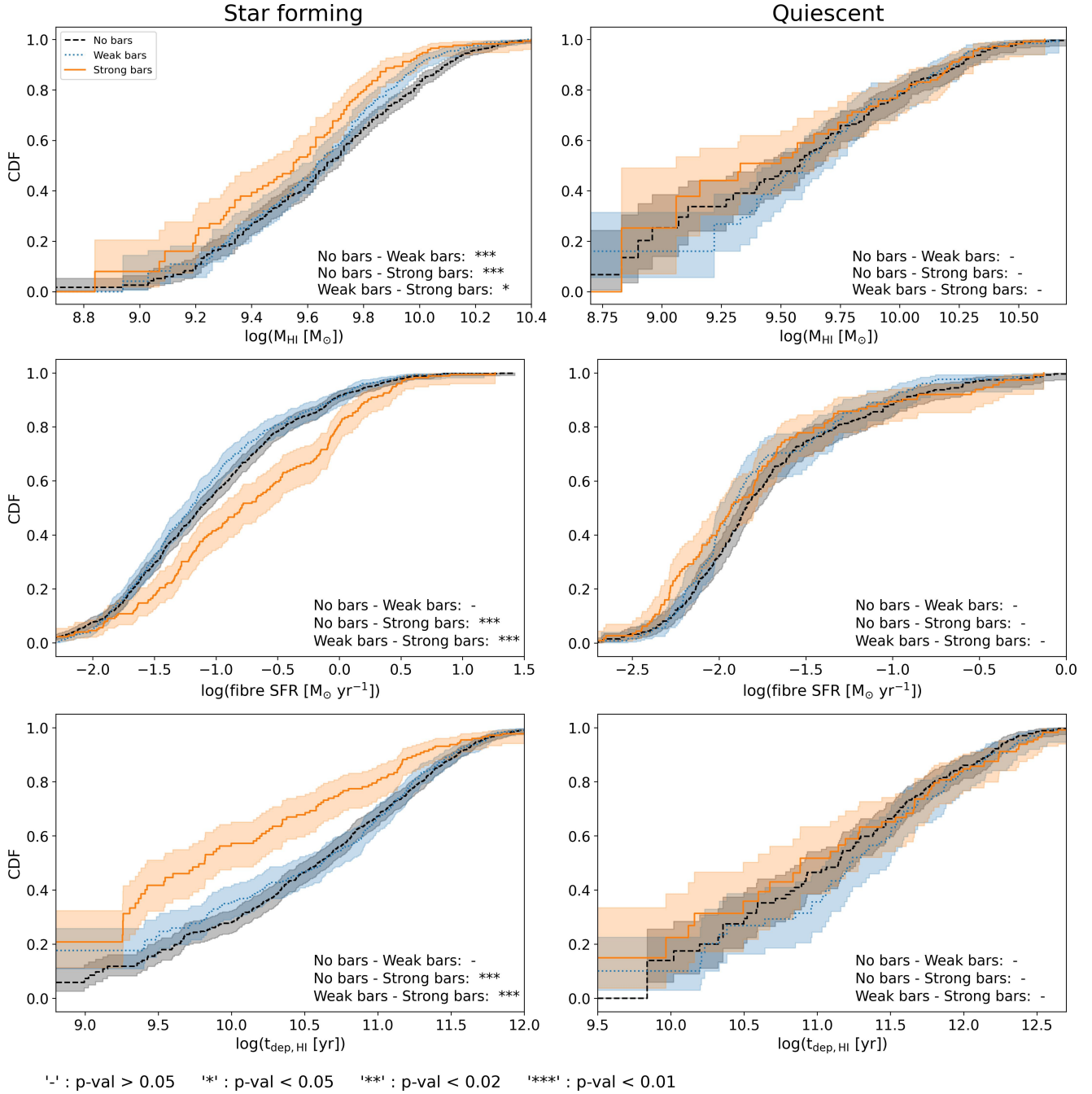


Figure 10. The results from a survival analysis on galaxies with no bar (black dashed), a weak bar (blue dotted) and a strong bar (orange full) in the SF group (left) and quiescent group (right). The top row displays the results for the HI gas mass, the middle row for fibre SFR and the depletion timescale is shown in the bottom row. The results are shown in the form of cumulative density functions (CDFs). The results of the Cox’s proportional hazards model are displayed in the bottom-right corner of every panel. If the p-value is below 0.01 (i.e., they are distinct), it is marked with ‘***’. If the p-value was between 0.01 and 0.02, it is denoted with ‘**’. If it was between 0.02 and 0.05, ‘*’ was used. If it is above 0.05, it was denoted with ‘-’. The SF galaxies with a strong bar are statistically significantly different from SF galaxies with a weak bar or no bar, especially in terms of fibre SFR and depletion timescale. Strong bars in SF galaxies have the highest fibre SFRs and shortest depletion timescales. There are no significant differences among the bar types in the quiescent galaxies.

SFR positively correlates with bar length (absolute and relative), suggesting that the strongest and longest bars have the highest fibre SFR and affect their host the most. This is not the case for the quiescent galaxies.

This leads us to ask a more fundamental question: are strong and weak bars fundamentally distinct physical phenomena and dis-

tinct populations? Or are they just two labels we give to bars that are on opposite ends of a continuum of bar types? If strong and weak bars are distinct phenomena, then we expect to see differences between the two bar types when controlling for bar length. The results of Figure 12 give weight to the latter option, as it shows that, for a

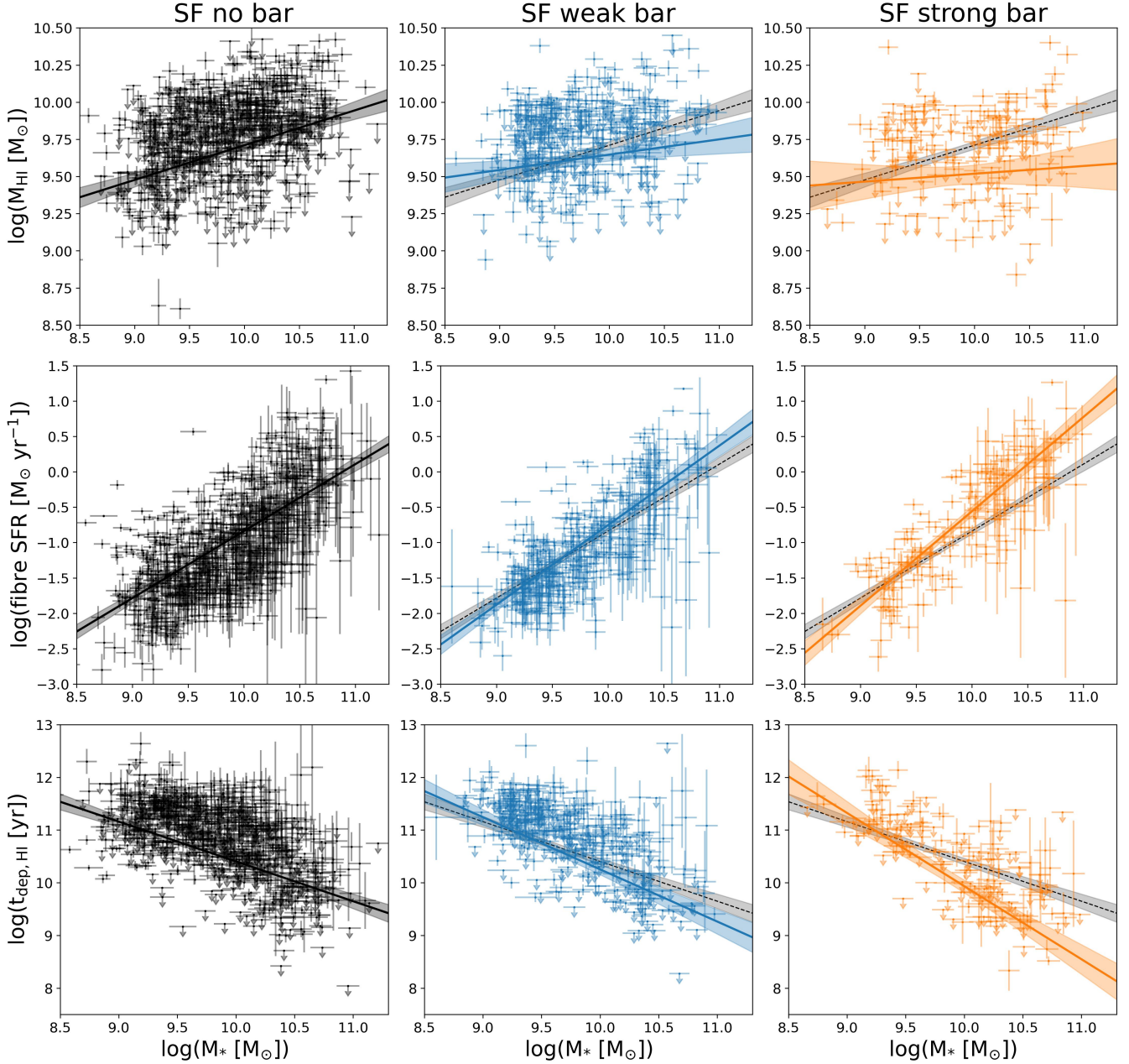


Figure 11. One-dimensional trends between HI gas mass (top row), fibre SFR (middle row) and depletion timescale (bottom row) and stellar mass. The trends were assessed using the linnmix Python package, which is based on the hierarchical Bayesian model of Kelly (2007). The fits were created separately for SF galaxies with no bar (left column), SF galaxies with a weak bar (middle column) and SF galaxies with a strong bar (right column). The trends of the unbarred galaxies are drawn over the other panels as well (in black, dashed) to facilitate comparison. The 2σ errors on the fit are displayed with the light shading. The trends of the SF galaxies with a weak bar seem very similar to the trends of the SF unbarred galaxies. In contrast, the trends of the SF galaxies with a strong bar are very different from that of the SF unbarred galaxies: the SF galaxies with a strong bar have lower gas mass, high fibre SFRs and shorter depletion timescales than SF unbarred galaxies, except at the lowest stellar masses.

given bar length (absolute or relative), there is no difference in fibre SFR.

We can see that the GZD bar vote fractions correctly reflect the continuous nature of bar types. In Figure 13, we plot the vote fractions ($p_{\text{no bar}}$, $p_{\text{weak bar}}$ and $p_{\text{strong bar}}$) against bar length. These results show that, as the bar becomes longer (both absolute and relative length), volunteers are more likely to vote that the bar is strong. This is not surprising, as we tell the volunteers that strong

bars are longer. However, this figure also shows that volunteers become increasingly confident that a bar is strong if it is longer. After a bar length of ~ 6 kpc (or a relative bar length of $\sim 35\%$), we start to see more strong than weak bars. However, there is no distinctive bar length cut-off before (after) which a bar is always weak (strong). This emphasizes the continuous nature of bar types, rather than the dichotomy that separates weak and strong bars in distinct separate classes.

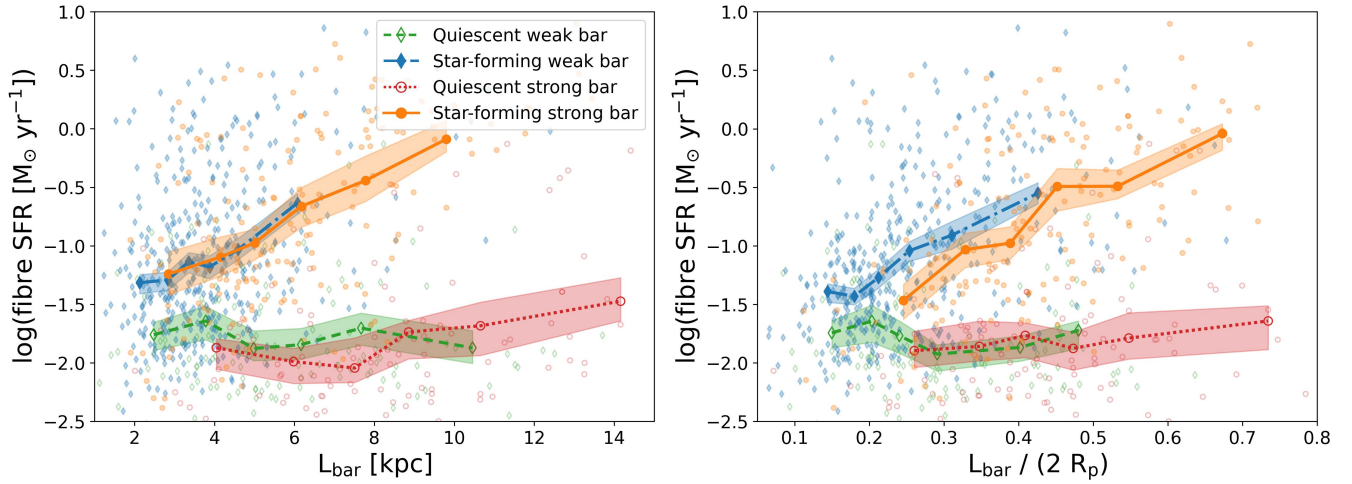


Figure 12. Left: The absolute bar length (in kpc) against fibre SFR for quiescent galaxies with a weak bar, quiescent galaxies with a strong bar, SF galaxies with a weak bar and SF galaxies with a strong bar. **Right:** The relative bar length (obtained by dividing the absolute length by the SDSS r-band Petrosian diameter) against fibre SFR. Please refer to Figure 9 for histograms of the bar lengths. At a given bar length (absolute or relative), the fibre SFR for SF galaxies with a strong bar is not higher than the fibre SFR for SF galaxies with a weak bar, contrary to what was observed in Figures 10 and 11. The contours represent the 3σ region after bootstrapping the data 10,000 times and retaining 90% of the data for each iteration.

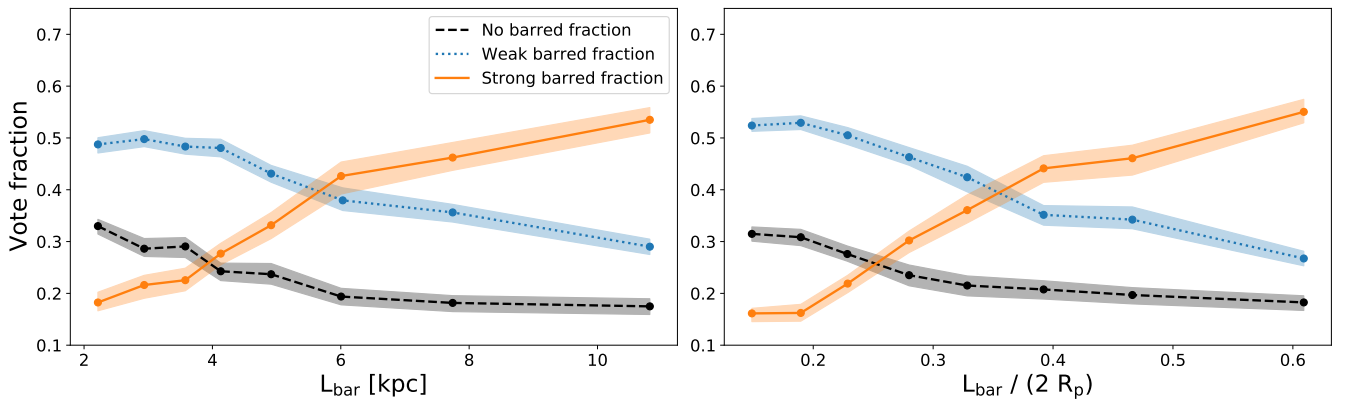


Figure 13. Left: The absolute bar length (in kpc) against the average strong, weak and unbarred vote fraction. **Right:** The relative bar length (obtained by dividing the absolute length by the SDSS r-band Petrosian diameter). Volunteers become increasingly confident that a bar is strong if it is longer. The contours represent the 3σ region after bootstrapping the data 10,000 times and retaining 90% of the data for each iteration.

In Figure 14, we show postage stamps of randomly selected galaxies in the intermediate relative bar length ($L_{\text{bar}}/\text{Petrosian}$) region where there are both strong and weak bars ($0.27 < L_{\text{bar}}/\text{Petrosian} < 0.37$). The top row shows bars that are classified as strong bars by GZD, while the bottom row shows weak bars. Around 23% (188 out of 814) of the barred galaxies in our sample fall within this intermediate relative bar length range. After visual inspection of those galaxies, it seems clear that morphologically speaking, galaxies with strong and weak bars of intermediate relative length look very similar to each other, unlike the obviously strong and weak bars shown previously in Figure 3.

These results show that at an intermediate relative bar length (absolute or relative), strong and weak bars seem to be hard to differentiate. This suggests that strong and weak bars are not distinct physical phenomena and hints at the continuous nature of bar types.

4 DISCUSSION

4.1 Difference in bar length between strong and weak bars

In Figure 9 in Section 3.2, we compared the absolute bar length and relative bar length for weak and strong bars, separated into SF and quiescent subsamples. We see that strong bars are typically longer than weak bars (both in terms of absolute and relative size). This is expected, as this corresponds to the guidelines given to the volunteers while classifying. However, we also found that, when measuring the bar length in kpc (absolute size) quiescent galaxies have longer bars, regardless of bar type. Bars in quiescent galaxies are, on average, longer than bars in SF galaxies, for both weak and strong bars. This can be explained by supposing that bars in SF galaxies have not reached their full size yet and are still growing, whereas bars in quiescent galaxies have reached their maximum size and cannot grow anymore.

This difference disappears when measuring the bar size relative

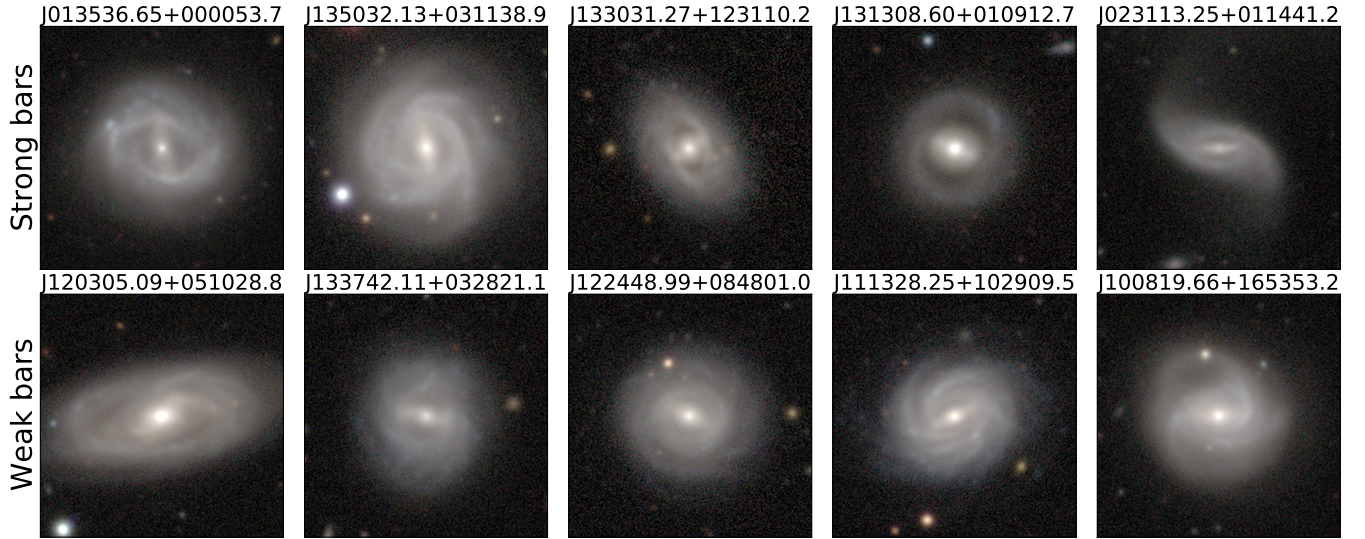


Figure 14. DECaLS postage stamps (59x59 arcsec) of galaxies with intermediate relative bar lengths ($0.27 < L_{\text{bar}}/\text{Petrorad} < 0.37$) and redshifts between $0.027 < z < 0.035$. Galaxies classified by GZD as having a strong bar are shown in the top row, while galaxies with a weak bar are in the bottom row. About 23% of the bars in our sample fall within this intermediate relative bar length range. The authors of this paper find it hard to distinguish between the weak and strong bars presented here, especially considering the obvious morphological differences between weak and strong bars in Figure 3.

to the Petrosian diameter. Strong bars typically cover 40–45% of the Petrosian diameter, whereas weak bars only cover around 20–30%, regardless whether the host is SF or quiescent. This observation hints that bars do not evolve independently from their host.

However, it is possible that the observed results are a simple consequence of quiescent galaxies being bigger than SF galaxies and that volunteers classify bars into weak or strong based on the relative bar length (as we expect them to). This possibility is discussed in more detail in Appendix C. While the interpretation is open to debate, we can conclude that in terms of absolute bar length, bars in quiescent galaxies are longer than bars in SF galaxies, irrespective of bar type. In addition, we found that in terms of relative bar length, strong bars cover 40–45% of the Petrosian diameter, while weak bars cover 20–30%, irrespective of whether the host galaxy is quiescent or SF.

4.2 Strong bars are more common among quiescent galaxies

In Figure 6 in Section 3.1.1, we looked at the properties of the galaxies hosting bars. We showed that the strong bar fraction increases monotonically with (g-r) colour and stellar mass. The strong bar fraction is also highest at lower SFR bins, although there is a significant population of strong bars found at higher SFR (and fibre SFRs). This is in agreement with the literature, as many other studies have shown that bars are more likely to be found in galaxies that have higher stellar mass, less gas, redder colours and low SFRs (Nair & Abraham 2010b; Masters et al. 2012; Vera et al. 2016; Cervantes Sodi 2017). However, we have only observed these results for strong bars, not weak bars.

Erwin (2018) showed that, in a sample drawn from the Spitzer Survey of Stellar Structure in Galaxies (S4G), the bar fraction is constant over a range of (g-r) colours and gas fractions. Their bar fraction does not increase, but rather decreases for stellar masses higher than $\sim 10^{9.7} M_{\odot}$. These results are in contrast to many SDSS-based studies cited above. Erwin (2018) argues that this apparent contradiction can be explained if SDSS-based studies miss bars in

low-mass blue galaxies. In Figures 5 and 6, we showed that the newly detected bars in GZD (compared to GZ2) are weak bars in low-mass blue galaxies. Nevertheless, the ‘combined’ bar fraction in Figure 6 is not constant over (g-r) colour and agrees well with Masters et al. (2011) for redder colours ((g-r) colour > 0.5). Additionally, our ‘combined’ bar fraction remains roughly constant over stellar mass. As mentioned before, we conclude that strong bars drive the trends of bar fraction with (g-r) colour, stellar mass and SFR observed in other studies (Nair & Abraham 2010b; Masters et al. 2011, 2012; Vera et al. 2016; Cervantes Sodi 2017). However, the addition of weak bars in low-mass blue galaxies is insufficient to resolve the apparent disagreement between Erwin (2018) and many SDSS-based studies (Masters et al. 2011, 2012; Vera et al. 2016; Cervantes Sodi 2017; Kruk et al. 2018), which instead seems likely to be due to the very different sample selection of the S4G and SDSS galaxy samples. For example, the median stellar mass of the sample used in Erwin (2018) is $\sim 10^{9.6} M_{\odot}$ (based on their Figure 4 and the bins in the top-left panel of their Figure 5). However, the median stellar mass of our sample is $10^{10.6} M_{\odot}$. As stellar mass correlates with many parameters (including bar length), this can have major consequences. Additionally, as Erwin (2018) notes, there is also the issue of resolution to consider. With an r-band FWHM of 1.18" from DECaLS (Dey et al. 2019) and a mean redshift of 0.036, the mean linear resolution of our sample is approximately 834 pc, which is higher than the 165 pc of Erwin (2018). This explains why they observe many sub-kpc bars, while we do not. These differences in stellar mass and resolution will manifest themselves in the conclusions, so a more detailed analysis is needed for a proper comparison with Erwin (2018).

In Figures 7 and 8 in Section 3.1.2, we observe higher strong bar fractions in the red sequence and in quiescent galaxies (24.9% and 22.0%, respectively) than in the blue cloud and in SF galaxies (9.6% and 13.0%, respectively). The fraction of galaxies with a weak bar is roughly the same in red sequence and in quiescent galaxies (25.2% and 25.0%, respectively) compared to the blue cloud and in SF galaxies (29.9% and 29.3%, respectively). This data can be

interpreted in two different ways. Either it is easier to form strong bars in quenched galaxies, or only strong bars help to quench the galaxy (Masters et al. 2012).

4.3 Strong bars in star forming galaxies facilitate quenching

In an attempt to see whether strong bars help to quench their host or if it is easier to form a strong bar in a quenched galaxy, we performed a detailed analysis on fibre SFR, HI gas mass and the depletion timescale in Figures 10 and 11 in Section 3.3. We found that, on average, SF galaxies with a strong bar have higher fibre SFRs, lower gas masses and shorter depletion timescales for a given stellar mass, compared to SF unbarred galaxies. This suggests that, on average, SF galaxies with a strong bar are more rapidly evolving galaxies and are more efficient in star formation, compared to unbarred galaxies. In contrast, SF galaxies with a weak bar do not differ significantly from galaxies without bars in terms of fibre SFR and depletion timescale. Similarly, no significant differences were observed between quiescent galaxies with a strong, weak or no bar. Do note that we are describing average properties and that there is scatter around these trends. A particular weakly barred galaxy can still have a higher fibre SFR than another galaxy with a strong bar. However, on average, the trends described above apply.

It has been suggested before by various other authors that bars can affect and potentially quench their host through “secular evolution” (Kormendy & Kennicutt 2004; Sheth et al. 2005; Athanassoula 2007; Masters et al. 2011; Cheung et al. 2013; Kruk et al. 2018; Efthymiopoulos et al. 2019). This can be done by bars funnelling gas inwards (Athanassoula 1992b; Athanassoula et al. 2013; Villa-Vargas et al. 2010) and once the gas is concentrated in the centre, it is used to increase SFR. Increasing the SFR in a galaxy speeds up the rate of gas consumption, thereby facilitating the transition from star forming to quenched. An increase in SFR in barred galaxies has been observed before (Alonso-Herrero & Knapen 2001; Hunt et al. 2008; Ellison et al. 2011; Coelho & Gadotti 2011; Hirota et al. 2014; Janowiecki et al. 2020; Magaña-Serrano et al. 2020; Lin et al. 2020). However, we conclude that, on average, **only strong bars in SF galaxies help to quench their host through secular evolution.**

We have observed an increase in fibre SFR for SF galaxies with a strong bar, meaning within the central 3 arcsecs of the galaxy. Further constraining the spatial distribution of the observed increase in SFR is of much interest and could be done with integral field spectroscopic surveys such as Mapping Nearby Galaxies at Apache Point Observatory (MaNGA, Bundy et al. 2015). As Gavazzi et al. (2015) note, a bar only helps to quench the inner regions of a galaxy, which gives the bar its usual red colour. A similar phenomena is found in the ‘star formation desert’ by James & Percival (2018) as well as the observed gas-depleted regions in barred galaxies Spinoso et al. (2017); George et al. (2019); Newnham et al. (2020). Thus, other quenching mechanisms, such as environmental quenching, are likely to be needed to work in tandem with bar quenching in order to fully quench the galaxy (Smethurst et al. 2017).

Nevertheless, some studies have shown that bars do not cause an increase of SFR/SFE (Sheth et al. 2000; Khoperskov et al. 2018). Watanabe et al. (2011) found that within the bar radius the SFE is similar to the disk region. Even more, Sheth et al. (2000) found lower SFR in the region between the centre and bar ends. These lower SFR/SFE in strongly barred regions have been explained by strong gas flow and/or shear effects induced by the bar potential, which lowers SFR (Athanassoula 1992b; Reynaud & Downes 1998; Sheth et al. 2000; Sorai et al. 2012; Meidt et al. 2013; Momose et al. 2010; Nimori et al. 2013; Krishnarao et al. 2020) or fast

cloud-cloud collisions (Fujimoto et al. 2014; Maeda et al. 2018; Fujimoto et al. 2020; Maeda et al. 2021). In contrast to the studies cited above, we see an increase in fibre SFR. However, the fibre only covers the central 3 arcsec of every galaxy, which corresponds to the central 0.69 - 2.93 kpc in our sample. As shown in Figure 9 in Section 3.2, bars (especially strong bars) are typically larger than that, which means that the fibre only covers the central part of the bar. This suggests that the increase in SFR observed here is indicative of an increase in SFR in the centre of the galaxy, and not in the entire bar or bar-end region, which is where the studies cited above typically look at. Additionally, many of these studies do not differentiate between weak and strong bars, which could also explain the apparent discrepancy, as we have only found an increase in fibre SFR in SF galaxies with a strong bar.

We have provided evidence that SF strong bars help to quench their host. However, the simulations of Athanassoula et al. (2013) found that a bar starts forming later and forms more slowly if the gas fraction is high. At the end of their simulation, the bar was much weaker in gas-rich galaxies. This is a recurring finding (Villa-Vargas et al. 2010; Cervantes Sodi 2017). Sheth et al. (2008) has shown that at high redshifts, red disk galaxies obtain their bar earlier than blue spirals. These findings would suggest that it is easier to form bars in quenched galaxies, not that bars facilitate quenching. However, it is important to note that our results do not exclude this possibility. Instead, our results suggest that SF strong bars facilitate quenching, and it may still be true that strong bars are easier to form in quenched galaxies at the same time.

4.4 Are weak and strong bars different phenomena?

After having established that, on average, SF galaxies with a strong bar have higher fibre SFRs than SF galaxies with a weak bar for any given stellar mass, we have shown that this is not true when controlling for bar length in Figure 12 in Section 3.4. In other words, in terms of fibre SFR, weak and strong bars of a fixed bar length are indiscriminable. This compelled us to look at images of weak and strong bars in galaxies that have ‘intermediate’ bar lengths ($0.27 < L_{\text{bar}}/L_{\text{Petrord}} < 0.37$) in Figure 14 and concluded that they look very similar.

If weak and strong bars were physically different phenomena, we would expect to see differences in fibre SFR at a fixed bar length. As we did not see any, we have to conclude that weak and strong bars are not separate and distinct barred phenomena. Rather, we propose that all barred galaxies are part of a continuum of bar types, which have previously been divided into two populations (weak and strong). With this continuum in mind, it makes more sense to talk about ‘stronger’ and ‘weaker’ bars, rather than ‘strong’ and ‘weak’ bars.

Even though one of the conclusions of this paper is that weak and strong bars are not fundamentally distinct physical phenomena, we believe it is still worthwhile to characterise and differentiate between the ends of that continuum, as the extremes do have varying effects on their host (e.g. in fibre SFR, gas mass and depletion timescale). This is most easily done by splitting the bar population into two or more categories, as done by GZD (weak and strong) and Nair & Abraham (2010a) (weak, intermediate and strong). One should only be cautious while choosing a threshold and should keep the continuous nature of bar types in mind while interpreting the results.

The proposed bar continuum is visualised in Figure 15 using DECaLS postage stamps. The galaxies are ordered from having weaker bars to stronger bars (from left to right). In this paper, we

have shown that various parameters scale with this bar continuum on a population level, such as bar length (absolute and relative) and stellar mass. When we only consider SF galaxies, we have also shown that only the strongest bars increase the fibre SFR, decrease HI gas mass and lower the depletion timescale, which facilitates the quenching process. This is not observed for weaker bars and illustrates how the position of the bar on this continuum can have a big effect on the host galaxy.

Multiple studies have found that bars can grow longer and stronger over time (Athanasoulas 2003; Kim et al. 2015, 2016; Díaz-García et al. 2016; Algorry et al. 2017). This implies that, in the context of the bar continuum, bars will move over this continuum over time.

Other studies have suggested that there are differences in the surface brightness profile of weak and strong bars. Weaker bars tend to have exponential profiles, whereas stronger bars have flatter profiles (Elmegreen & Elmegreen 1985; Elmegreen et al. 1996; Kim et al. 2015; Kruk et al. 2018). Furthermore, Kim et al. (2015) found a correlation with bar length as well: longer bars, on average, have flatter profiles. Kim et al. (2015) speculate that bars initially have an exponential profile, which evolves over time (by trapping more stars into bar orbits) to a flatter profile. This allows for surface brightness profiles in between exponential and flat, which fits nicely with our hypothesis of the continuous nature of bar types and suggests that the surface brightness profile of the bar scales according to our proposed bar continuum.

5 CONCLUSION

We have used the newest version of Galaxy Zoo, Galaxy Zoo DECaLS (GZD), to obtain a statistically significant and robust sample of 1,867 face-on disk galaxies with reliable bar classifications. The images used in GZD were obtained from the Dark Energy Camera Legacy Survey (DECaLS, Dey et al. 2019). Using the classification scheme shown in Table 1, we found that 28.1% of all our galaxies are classified as having a weak bar, while 15.5% are classified as having a strong bar. This results in a total barred fraction of 43.6%. We combined this data with SFR and stellar mass measurements from MPA-JHU (Kauffmann et al. 2003; Brinchmann et al. 2004; Tremonti et al. 2004) and gas mass measurements from ALFALFA (Giovannelli et al. 2005; Haynes et al. 2011, 2018) to conduct a study looking at the differences between strong and weak bars for the first time.

Our sample is consistent with the catalogue of visual morphological classifications of Nair & Abraham (2010a) as well as with GZ2. We do measure a higher total barred fraction with GZD compared to GZ2, due to an improved decision tree and deeper imaging. Nevertheless, GZ2 did detect most GZD strong bars. Most of the newly detected bars in GZD (compared with GZ2) are weak bars.

In addition, we saw that strong bars are longer than weak bars in terms of both the absolute and relative bar length. The average strong bars covers 40-45% of their host galaxy, whereas the average weak bar covers only 20-30%, although there is still significant overlap. Bars in quiescent galaxies are longer (in absolute length) than bars in SF galaxies for both weak and strong bars.

However, most importantly, we have found that:

(i) *The strongest bars facilitate quenching in SF galaxies.*

- The strong bar fraction is higher in the red sequence and in quiescent galaxies (24.9% and 22.0%, respectively) than in the blue cloud and in SF galaxies (9.6% and 13.0%, respectively),

whereas the weak bar fraction is roughly similar in both the red sequence and quiescent galaxies (24.9% and 25.0%, respectively) and the blue cloud and in SF galaxies (29.9% and 29.3%, respectively)

- SF galaxies with a stronger bar have, on average, significantly higher fibre SFRs, lower gas masses and shorter depletion timescales than unbarred SF galaxies for a given stellar mass. This highlights that SF galaxies with stronger bars are usually rapidly evolving galaxies and that the strong bar facilitates the quenching process in these galaxies. These differences were not observed between SF galaxies with a weaker bar and SF unbarred galaxies.

- Quiescent galaxies with weaker and stronger bars do not significantly differ from quiescent galaxies with no bar.

(ii) *Weak and strong bars are part of a continuum of bar types.*

- We have found that weak and strong bars are not fundamentally distinct physical phenomena, as we have shown that all differences between weak and strong bars disappear when controlling for bar length. Thus, there exists a continuum of bar types, for which weak and strong are the labels given to the extremes of this continuum.

- Nevertheless, it is still worthwhile to try to classify stronger and weaker bars into separate categories. This is because the effects that the bar exerts on its host depends on its position on the continuum. However, one must be cautious when doing so and be aware that results obtained by splitting bars into groups will only probe the extremes of the continuum.

ACKNOWLEDGEMENTS

The data in this paper are the result of the efforts of the Galaxy Zoo volunteers, without whom none of this work would be possible. Their efforts are individually acknowledged at <http://authors.galaxyzoo.org>.

TG gratefully acknowledges funding from the University of Oxford Department of Physics and the Saven Scholarship.

RJS gratefully acknowledges funding from Christ Church, University of Oxford.

Funding for the Sloan Digital Sky Survey IV has been provided by the Alfred P. Sloan Foundation, the U.S. Department of Energy Office of Science, and the Participating Institutions.

SDSS-IV acknowledges support and resources from the Center for High Performance Computing at the University of Utah. The SDSS website is www.sdss.org.

SDSS-IV is managed by the Astrophysical Research Consortium for the Participating Institutions of the SDSS Collaboration including the Brazilian Participation Group, the Carnegie Institution for Science, Carnegie Mellon University, Center for Astrophysics | Harvard & Smithsonian, the Chilean Participation Group, the French Participation Group, Instituto de Astrofísica de Canarias, The Johns Hopkins University, Kavli Institute for the Physics and Mathematics of the Universe (IPMU) / University of Tokyo, the Korean Participation Group, Lawrence Berkeley National Laboratory, Leibniz Institut für Astrophysik Potsdam (AIP), Max-Planck-Institut für Astronomie (MPIA Heidelberg), Max-Planck-Institut für Astrophysik (MPA Garching), Max-Planck-Institut für Extraterrestrische Physik (MPE), National Astronomical Observatories of China, New Mexico State University, New York University, University of Notre Dame, Observatório Nacional / MCTI, The Ohio

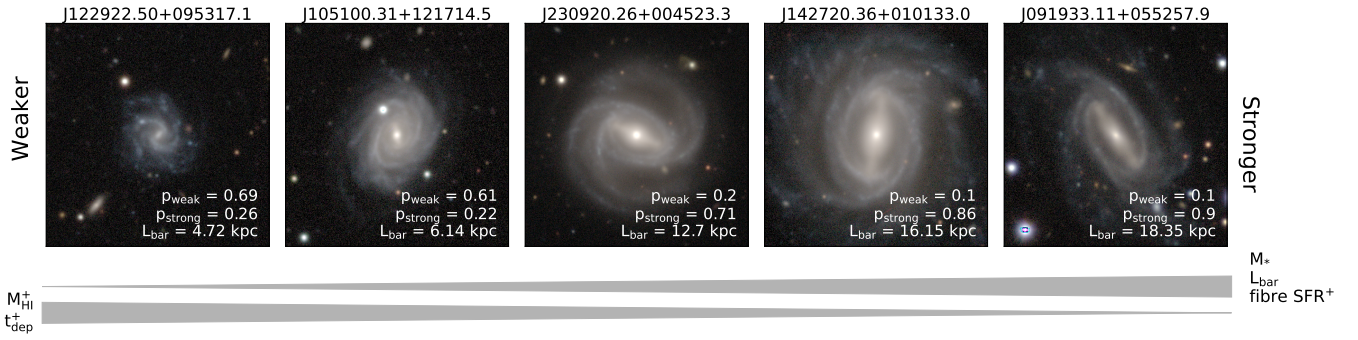


Figure 15. A visualisation of the proposed bar continuum with DECaLS postage stamps (93x93 arcsec). The continuum is shown going from weaker bars (left) to stronger bars (right). Various parameters scale together with this continuum. For example: bar length (absolute and relative), p_{strong} , stellar mass and fibre SFR. Conversely, various parameters are inversely proportional to bar strength, such as p_{weak} , HI gas mass and depletion timescale. Please note that depletion timescale, HI gas mass and fibre SFR only show these trends if we only consider SF galaxies (denoted by the plus sign in superscript). The bar continuum shown here is based on the absolute bar length (L_{bar}), but it can also be based on other parameters, such as relative bar length or a combination of p_{weak} and p_{strong} .

State University, Pennsylvania State University, Shanghai Astronomical Observatory, United Kingdom Participation Group, Universidad Nacional Autónoma de México, University of Arizona, University of Colorado Boulder, University of Oxford, University of Portsmouth, University of Utah, University of Virginia, University of Washington, University of Wisconsin, Vanderbilt University, and Yale University.

The Legacy Surveys consist of three individual and complementary projects: the Dark Energy Camera Legacy Survey (DECaLS; Proposal ID #2014B-0404; PIs: David Schlegel and Arjun Dey), the Beijing-Arizona Sky Survey (BASS; NOAO Prop. ID #2015A-0801; PIs: Zhou Xu and Xiaohui Fan), and the Mayall z-band Legacy Survey (MzLS; Prop. ID #2016A-0453; PI: Arjun Dey). DECaLS, BASS and MzLS together include data obtained, respectively, at the Blanco telescope, Cerro Tololo Inter-American Observatory, NSF’s NOIRLab; the Bok telescope, Steward Observatory, University of Arizona; and the Mayall telescope, Kitt Peak National Observatory, NOIRLab. The Legacy Surveys project is honored to be permitted to conduct astronomical research on Iolkam Du’ag (Kitt Peak), a mountain with particular significance to the Tohono O’odham Nation.

The authors would like to thank the ALFALFA team for observing and processing of the ALFALFA data set.

This research made use of Astropy,⁴ a community-developed core Python package for Astronomy (Astropy Collaboration et al. 2013, 2018), as well as other Python packages, such as Matplotlib (Hunter 2007), NumPy (Harris et al. 2020), linmix⁵, lifelines (Davidson-Pilon et al. 2021), pandas (Wes McKinney 2010; pandas development team 2020) and SciPy (Virtanen et al. 2020).

This research made use of TOPCAT (Taylor 2005).

DATA AVAILABILITY

The GZD data used in this article is made publicly available via Zenodo at <https://dx.doi.org/10.5281/zenodo.4196267>. The DECaLS DR8 data can be found at <https://www.legacysurvey.org/dr8/>. The latest SDSS data can be found at <https://www.sdss.org/dr16/>.

⁴ <http://www.astropy.org>

⁵ <http://linmix.readthedocs.org/>

The MPA-JHU VAC can be found at <https://www.mpa.mpg.de/SDSS/DR7/>. The ALFALFA data used in this article can be found at <http://egg.astro.cornell.edu/>.

REFERENCES

- Abazajian K. N., et al., 2009, *ApJS*, **182**, 543
Adelman-McCarthy J. K., et al., 2008, *ApJS*, **175**, 297
Aguerre J. A. L., Méndez-Abreu J., Corsini E. M., 2009, *A&A*, **495**, 491
Ahumada R., et al., 2020, *ApJS*, **249**, 3
Algorry D. G., et al., 2017, *MNRAS*, **469**, 1054
Alonso-Herrero A., Knapen J. H., 2001, *AJ*, **122**, 1350
Astropy Collaboration et al., 2013, *A&A*, **558**, A33
Astropy Collaboration et al., 2018, *AJ*, **156**, 123
Athanasoulas E., 1992a, *MNRAS*, **259**, 328
Athanasoulas E., 1992b, *MNRAS*, **259**, 345
Athanasoulas E., 2003, *MNRAS*, **341**, 1179
Athanasoulas E., 2007, *Astrophysics and Space Science Proceedings*, **3**, 195
Athanasoulas E., Machado R. E. G., Rodionov S. A., 2013, *MNRAS*, **429**, 1949
Barazza F. D., Jogee S., Marinova I., 2008, *ApJ*, **675**, 1194
Belfiore F., et al., 2018, *MNRAS*, **477**, 3014
Blanton M. R., et al., 2017, *AJ*, **154**, 28
Brinchmann J., Ellis R. S., 2000, *ApJ*, **536**, L77
Brinchmann J., Charlot S., White S. D. M., Tremonti C., Kauffmann G., Heckman T., Brinkmann J., 2004, *MNRAS*, **351**, 1151
Bundy K., et al., 2015, *ApJ*, **798**, 7
Buta R. J., 2011, arXiv e-prints, p. arXiv:1102.0550
Buta R., Block D. L., 2001, *ApJ*, **550**, 243
Buta R. J., Corwin H. G., Odewahn S. C., 2007, *The de Vaucouleurs Atlas of Galaxies*
Buta R. J., et al., 2019, *MNRAS*, **488**, 2175
Carles C., Martel H., Ellison S. L., Kawata D., 2016, *MNRAS*, **463**, 1074
Cervantes Sodi B., 2017, *ApJ*, **835**, 80
Cheung E., et al., 2013, *ApJ*, **779**, 162
Cheung E., et al., 2015, *MNRAS*, **447**, 506
Coelho P., Gadotti D. A., 2011, *ApJ*, **743**, L13
Combes F., Sanders R. H., 1981, *A&A*, **96**, 164
Cox D. R., 1972, *Journal of the Royal Statistical Society. Series B (Methodological)*, **34**, 187
Davidson-Pilon C., et al., 2020, *CamDavidsonPilon/lifelines*: v0.25.4, doi:10.5281/zenodo.4002777, <https://doi.org/10.5281/zenodo.4002777>
Davidson-Pilon C., et al., 2021, *CamDavidsonPilon/lifelines*: v0.25.9

- doi:10.5281/zenodo.4505728, <https://doi.org/10.5281/zenodo.4505728>
- Davoust E., Contini T., 2004, *A&A*, **416**, 515
- Dey A., et al., 2019, *AJ*, **157**, 168
- Díaz-García S., Salo H., Laurikainen E., Herrera-Endoqui M., 2016, *A&A*, **587**, A160
- Efthymiopoulos C., Kyziropoulos P. E., Pérez R. I., Zouloumi K., Gravvanis G. A., 2019, *MNRAS*, **484**, 1487
- Ellison S. L., Nair P., Patton D. R., Scudder J. M., Mendel J. T., Simard L., 2011, *Monthly Notices of the Royal Astronomical Society*, **416**, 2182–2192
- Elmegreen B. G., Elmegreen D. M., 1985, *ApJ*, **288**, 438
- Elmegreen B. G., Elmegreen D. M., Chromey F. R., Hasselbacher D. A., Bissell B. A., 1996, *AJ*, **111**, 2233
- Erwin P., 2004, *A&A*, **415**, 941
- Erwin P., 2018, *MNRAS*, **474**, 5372
- Eskridge P. B., et al., 2000, *AJ*, **119**, 536
- Flaugher B., et al., 2015, *AJ*, **150**, 150
- Fraser-McKelvie A., et al., 2020, *MNRAS*, **499**, 1116
- Fujimoto Y., Tasker E. J., Habe A., 2014, *MNRAS*, **445**, L65
- Fujimoto Y., Maeda F., Habe A., Ohta K., 2020, *MNRAS*, **491**, 4721
- Gadotti D. A., 2011, *MNRAS*, **415**, 3308
- Galloway M. A., et al., 2015, *MNRAS*, **448**, 3442
- García-Gómez C., Athanassoula E., Barberà C., Bosma A., 2017, *A&A*, **601**, A132
- Gavazzi G., et al., 2015, *A&A*, **580**, A116
- George K., Joseph P., Mondal C., Subramanian S., Subramaniam A., Paul K. T., 2019, *A&A*, **621**, L4
- Giovanelli R., et al., 2005, *AJ*, **130**, 2598
- Gunn J. E., et al., 1998, *AJ*, **116**, 3040
- Guo R., Mao S., Athanassoula E., Li H., Ge J., Long R. J., Merrifield M., Masters K., 2019, *MNRAS*, **482**, 1733
- Harris C. R., et al., 2020, *Nature*, **585**, 357
- Hart R. E., et al., 2016, *MNRAS*, **461**, 3663
- Haynes M. P., et al., 2011, *AJ*, **142**, 170
- Haynes M. P., et al., 2018, *ApJ*, **861**, 49
- Haywood M., Lehnert M. D., Di Matteo P., Snaith O., Schultheis M., Katz D., Gómez A., 2016, *A&A*, **589**, A66
- Hirota A., et al., 2014, *PASJ*, **66**, 46
- Hoyle B., et al., 2011, *MNRAS*, **415**, 3627
- Hubble E. P., 1926, *ApJ*, **64**, 321
- Hubble E. P., 1936, *Realm of the Nebulae*
- Hunt L. K., et al., 2008, *A&A*, **482**, 133
- Hunter J. D., 2007, *Computing in Science & Engineering*, **9**, 90
- James P. A., Percival S. M., 2018, *MNRAS*, **474**, 3101
- Janowiecki S., Catinella B., Cortese L., Saintonge A., Wang J., 2020, *MNRAS*, **493**, 1982
- Jogee S., Scoville N., Kenney J. D. P., 2005, *ApJ*, **630**, 837
- Kannappan S. J., et al., 2013, *ApJ*, **777**, 42
- Kauffmann G., et al., 2003, *MNRAS*, **341**, 33
- Kelly B. C., 2007, *ApJ*, **665**, 1489
- Kennicutt Robert C. J., 1998a, *ARA&A*, **36**, 189
- Kennicutt Robert C. J., 1998b, *ApJ*, **498**, 541
- Khoperskov S., Haywood M., Di Matteo P., Lehnert M. D., Combes F., 2018, *A&A*, **609**, A60
- Kim T., et al., 2015, *ApJ*, **799**, 99
- Kim T., Gadotti D. A., Athanassoula E., Bosma A., Sheth K., Lee M. G., 2016, *MNRAS*, **462**, 3430
- Kormendy J., Kennicutt Robert C. J., 2004, *ARA&A*, **42**, 603
- Krishnarao D., et al., 2020, *ApJ*, **898**, 116
- Kruk S. J., et al., 2017, *MNRAS*, **469**, 3363
- Kruk S. J., et al., 2018, *MNRAS*, **473**, 4731
- Kruk S. J., Erwin P., Debattista V. P., Lintott C., 2019, *MNRAS*, **490**, 4721
- Lara-López M. A., Bongiovanni A., Cepa J., Pérez García A. M., Sánchez-Portal M., Castañeda H. O., Fernández Lorenzo M., Pović M., 2010, *A&A*, **519**, A31
- Laurikainen E., Salo H., 2002, *MNRAS*, **337**, 1118
- Lin L., et al., 2020, *MNRAS*, **499**, 1406
- Lintott C. J., et al., 2008, *MNRAS*, **389**, 1179
- Lintott C., et al., 2011, *MNRAS*, **410**, 166
- Maeda F., Ohta K., Fujimoto Y., Habe A., Baba J., 2018, *PASJ*, **70**, 37
- Maeda F., Ohta K., Fujimoto Y., Habe A., 2020, *MNRAS*, **493**, 5045
- Maeda F., Ohta K., Fujimoto Y., Habe A., 2021, *MNRAS*, **502**, 2238
- Magaña-Serrano M. A., Hidalgo-Gómez A. M., Vega-Acevedo I., Castañeda H. O., 2020, *Rev. Mex. Astron. Astrofis.*, **56**, 39
- Masters K. L., et al., 2010, *MNRAS*, **405**, 783
- Masters K. L., et al., 2011, *MNRAS*, **411**, 2026
- Masters K. L., et al., 2012, *MNRAS*, **424**, 2180
- Meidt S. E., et al., 2013, *ApJ*, **779**, 45
- Melvin T., et al., 2014, *MNRAS*, **438**, 2882
- Menéndez-Delmestre K., Sheth K., Schinnerer E., Jarrett T. H., Scoville N. Z., 2007, *ApJ*, **657**, 790
- Momose R., Okumura S. K., Koda J., Sawada T., 2010, *ApJ*, **721**, 383
- Nair P. B., Abraham R. G., 2010a, *ApJS*, **186**, 427
- Nair P. B., Abraham R. G., 2010b, *ApJ*, **714**, L260
- Newham L., Hess K. M., Masters K. L., Kruk S., Penny S. J., Lingard T., Smethurst R. J., 2020, *MNRAS*, **492**, 4697
- Nimori M., Habe A., Sorai K., Watanabe Y., Hirota A., Namekata D., 2013, *MNRAS*, **429**, 2175
- Noeske K. G., et al., 2007, *ApJ*, **660**, L43
- Reynaud D., Downes D., 1998, *A&A*, **337**, 671
- Sandage A., 1961, *The Hubble Atlas of Galaxies*
- Sheth K., Regan M. W., Vogel S. N., Teuben P. J., 2000, *ApJ*, **532**, 221
- Sheth K., Vogel S. N., Regan M. W., Thornley M. D., Teuben P. J., 2005, *ApJ*, **632**, 217
- Sheth K., et al., 2008, *ApJ*, **675**, 1141
- Simmons B. D., et al., 2014, *MNRAS*, **445**, 3466
- Skibba R. A., et al., 2012, *MNRAS*, **423**, 1485
- Smethurst R. J., Lintott C. J., Bamford S. P., Hart R. E., Kruk S. J., Masters K. L., Nichol R. C., Simmons B. D., 2017, *MNRAS*, **469**, 3670
- Sorai K., et al., 2012, *PASJ*, **64**, 51
- Sorensen S. A., Matsuda T., Fujimoto M., 1976, *Ap&SS*, **43**, 491
- Speltinex T., Laurikainen E., Salo H., 2008, *MNRAS*, **383**, 317
- Spinoso D., Bonoli S., Dotti M., Mayer L., Madau P., Bellovary J., 2017, *MNRAS*, **465**, 3729
- Strauss M. A., et al., 2002, *AJ*, **124**, 1810
- Taylor M. B., 2005, in Shopbell P., Britton M., Ebert R., eds, *Astronomical Society of the Pacific Conference Series Vol. 347, Astronomical Data Analysis Software and Systems XIV*. p. 29
- Tremonti C. A., et al., 2004, *ApJ*, **613**, 898
- Vera M., Alonso S., Coldwell G., 2016, *A&A*, **595**, A63
- Villa-Vargas J., Shlosman I., Heller C., 2010, *ApJ*, **719**, 1470
- Virtanen P., et al., 2020, *Nature Methods*, **17**, 261
- Walmsley M., et al., 2021, in prep.
- Watanabe Y., Sorai K., Kuno N., Habe A., 2011, *MNRAS*, **411**, 1409
- Wes McKinney 2010, in Stéfan van der Walt Jarrod Millman eds, *Proceedings of the 9th Python in Science Conference*. pp 56 – 61, doi:10.25080/Majora-92bf1922-00a
- Willett K. W., et al., 2013, *MNRAS*, **435**, 2835
- Yajima Y., et al., 2019, *PASJ*, **71**, S13
- York D. G., et al., 2000, *AJ*, **120**, 1579
- Zhao D., Du M., Ho L. C., Debattista V. P., Shi J., 2020, *ApJ*, **904**, 170
- Zurita A., Relaño M., Beckman J. E., Knapen J. H., 2004, *A&A*, **413**, 73
- de Vaucouleurs G., 1959, *Handbuch der Physik*, **53**, 275
- de Vaucouleurs G., 1963, *ApJS*, **8**, 31
- de Vaucouleurs G., de Vaucouleurs A., Corwin Herold G. J., Buta R. J., Paturel G., Fouque P., 1991, *Third Reference Catalogue of Bright Galaxies*
- pandas development team T., 2020, *pandas-dev/pandas: Pandas*, doi:10.5281/zenodo.3509134, <https://doi.org/10.5281/zenodo.3509134>

APPENDIX A: COMPARISON TO NAIR AND ABRAHAM

We compared GZD to the catalogue of visual morphological classifications of Nair & Abraham (2010a) in section 2.5.2. We found that

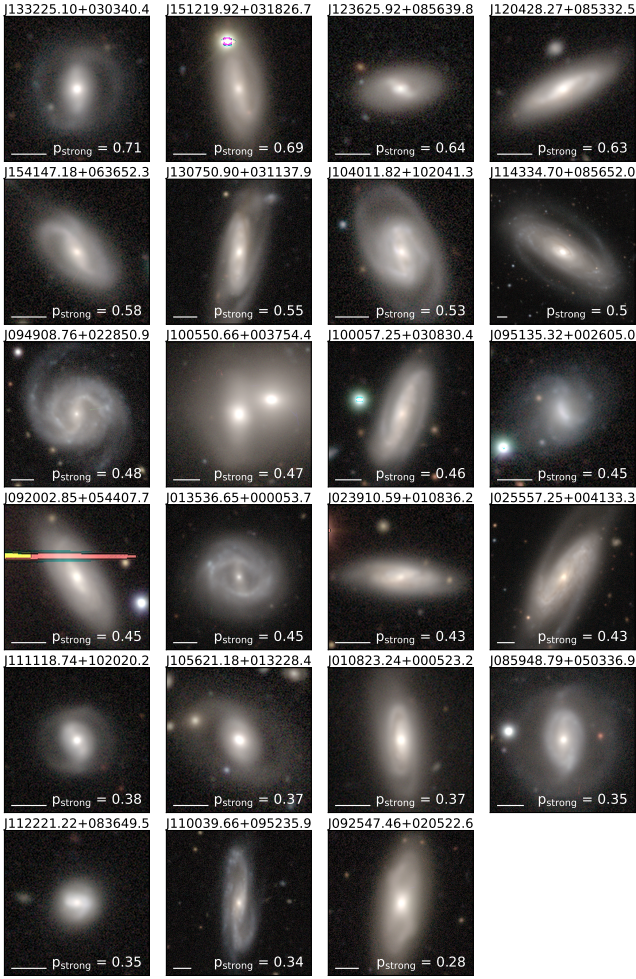


Figure A1. DECaLS postage stamps of the 23 galaxies classified by Nair & Abraham (2010a) as unbarred, while GZD classified them as having strong bars. The white horizontal line in the bottom left corner of each subplot is 10 arcsec long. The strong bar vote fraction ($p_{\text{strong bar}}$) of every galaxy is shown in the bottom right corner of each subplot. The galaxies are ordered from a high $p_{\text{strong bar}}$ (top left) to a low $p_{\text{strong bar}}$ (bottom right). The authors of this paper agree that the majority of these galaxies have a strong bar. The horizontal line over galaxy J092002.85+054407.7 is part of the mask of a very bright star just outside the frame.

there are 23 galaxies that Nair & Abraham (2010a) has classified as unbarred, whereas the same galaxies were classified by GZD as having a strong bar. Those galaxies are visualised in Figure A1.

The authors of this paper agree that the vast majority of these galaxies have a strong bar. The reason for this disagreement between Nair & Abraham (2010a) and GZD is most likely rooted in the different imaging used. GZD had access to DECaLS, while Nair & Abraham (2010a) used SDSS images.

APPENDIX B: EFFECT OF FIBRE SIZE

Throughout the paper, we have compared the fibre SFRs of galaxies with strong and weak bars. The fibre SFR probes the central 3 arcsec region of every galaxy. However, this 3 arcsec region will correspond to different physical distances depending on the redshift of the galaxy. We do not expect a change in the proportion of

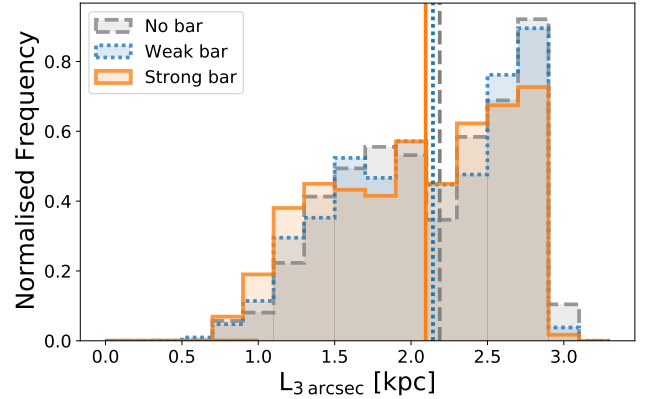


Figure B1. Histogram of the distribution of the physical distance corresponding to the 3 arcsec fibre ($L_{3 \text{ arcsec}}$) of the three bar types. The median value for every bar type is indicated with a dashed line. The three distributions do not significantly differ from each other (the results of a KS tests for the 3 comparisons are always $< 1.5\sigma$).

bar types over the short redshift range we are examining, but it is nevertheless worthwhile to investigate whether this will introduce a bias into our results. The distribution of the physical distance corresponding to the 3 arcsec fibre ($L_{3 \text{ arcsec}}$) for every bar type is visualised in Figure B1. The three distributions do not differ significantly from each other (KS test: all three $< 1.5\sigma$).

As a further test, we divided our sample into four $L_{3 \text{ arcsec}}$ bins and recreated the survival analysis plots for fibre SFR (similarly to Figure 10) for those different bins. The results are given in Figure B2.

Again, the quiescent group (right column) does not exhibit much difference between the different bar types, while the SF group (left column) does. Most of the differences are observed between SF galaxies with strong bars and the other bar types. Interestingly, we can see that at the highest $L_{3 \text{ arcsec}}$ bin (so at the highest redshifts), the differences are being ‘washed out’ by the surrounding areas that are now within the fibre. Nevertheless, our overall conclusions remain the same.

APPENDIX C: CO-EVOLUTION OF BAR AND GALAXY

In Section 3.2, we suggested that the bar could co-evolve with the galaxy, based on the bar length data shown in Figure 9. We saw that a strong bar in a SF galaxy tends to be shorter than a strong bar in a quiescent galaxy, and suggested that the bar co-evolves with its host and is still growing when in a SF galaxy and is fully grown once the host is quenched. Similar results were found for weak bars.

However, it is also possible that this result is obtained as direct consequence of the fact that volunteers classify based on the relative length of the bar, as instructed, and that quiescent galaxies tend to be bigger than SF galaxies.

This idea can be tested by temporarily stripping the weak/strong and quiescent/SF labels from each galaxy, and redistributing them according to the following rules: 1) quiescent galaxies are bigger and 2) strong bars are longer in terms of the relative size of the bar. To be more accurate, our sample was binned in eight equal-sized bins of Petrosian radius and for every bin we calculated what fraction of galaxies were quiescent (left plot of Figure C1). Then, when reassigning labels, the chance of labelling a particular

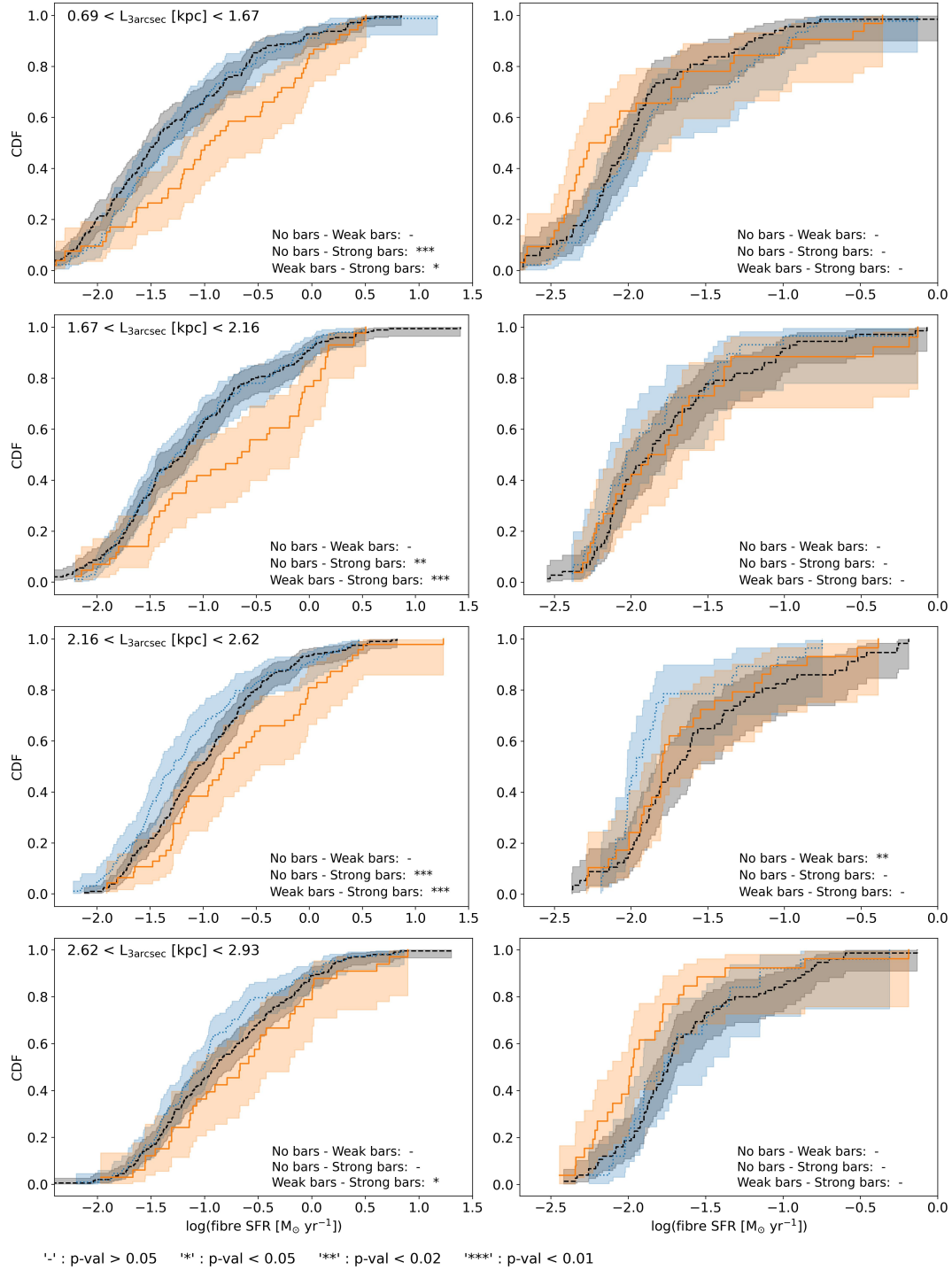


Figure B2. The results from a survival analysis on galaxies with no bar (black dashed) a weak bar (blue dotted) and a strong bar (orange full) in the SF group (left) and quiescent group (right). The galaxies are divided in four bins of $L_{3 \text{ arcsec}}$ (i.e., physical distance corresponding to the 3 arcsec fibre in kpc). The top row displays the results for the lowest $L_{3 \text{ arcsec}}$ bin and the bottom row the highest $L_{3 \text{ arcsec}}$ bin. The results are shown in the form of cumulative density functions (CDFs). The results of the Cox's proportional hazards model are displayed in the bottom-right corner of every panel. If the p-value is below 0.01 (i.e., they are distinct), it is marked with '***'. If the p-value was between 0.01 and 0.02, it is denoted with '**'. If it was between 0.02 and 0.05, '*' was used. If it is above 0.05, it was denoted with '-'.

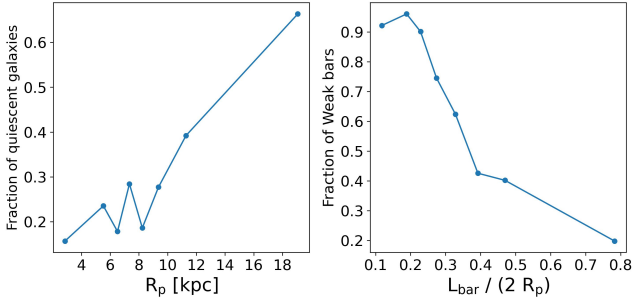


Figure C1. **Left:** The fraction of quiescent galaxies over Petrosian radius (R_p) in eight equal-size bins. These fractions are used for reassigning the quiescent/SF labels to the galaxies. **Right:** The fraction of weak bars over the relative size of the galaxy. These fractions are used for reassigning the weak/strong bar labels.

galaxy to be ‘quiescent’ was equal to that fraction. This was done as well for the relative bar length and the strong/weak bar labels (right plot of C1).

The result of doing this a 1,000 times per galaxy and plotting the bar length distribution for our four subsamples (quiescent galaxies with a weak bar, quiescent galaxies with a strong bar, SF galaxies with a weak bar and SF galaxies with a strong bar) is given in the top plot of Figure C2. As expected, the same trends that we saw in the observed data are found: a strong bar in a SF galaxy tends to be shorter than a strong bar in a quiescent galaxy (and similarly for weak bars). Although, the difference is not as large in the simulated results as in the observed results, shown in the bottom plot of Figure C2. Additionally, none of the observed distributions are likely drawn from their corresponding simulated distribution (p-value < 0.005 from a KS-test), except for the SF galaxies with a strong bar. Thus, there is still an unexplained effect, which is consistent with (but does not prove) the co-evolution theory described in Section 3.2.

This paper has been typeset from a \LaTeX file prepared by the author.

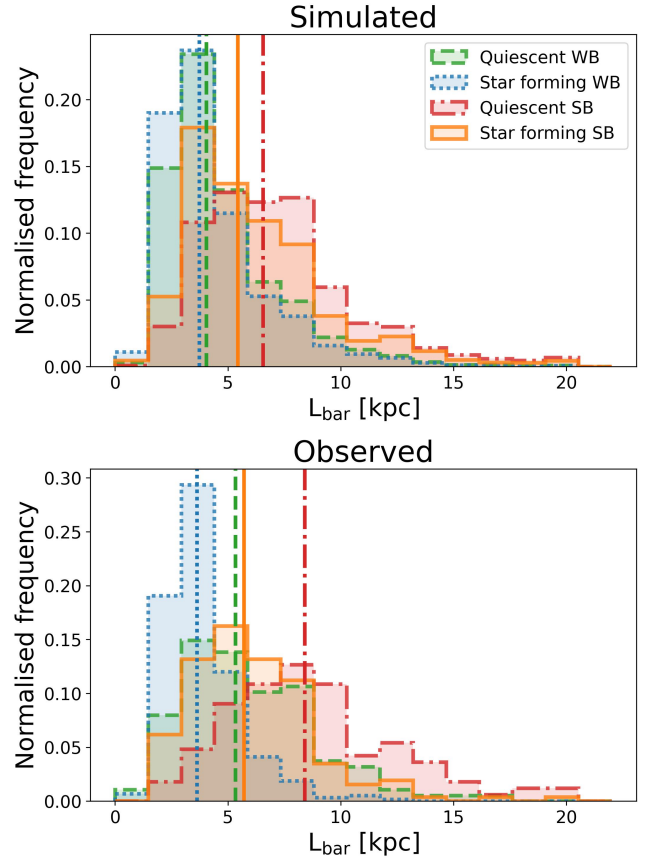


Figure C2. **Top:** The distribution of absolute bar lengths for the 1,000 different simulations for the four different subsamples: quiescent galaxies with a weak bar, quiescent galaxies with a strong bar, SF galaxies with a weak bar and SF galaxies with a strong bar. **Bottom:** The observed absolute bar lengths, identical to the left plot of Figure 9. As in the observed data, we see that a strong bar in a SF galaxy tends to be shorter than a strong bar in a quiescent galaxy in the simulation (and similarly for weak bars). However, the difference is bigger in the observed data than in the simulated data.